

NACA RM L52J21a

7375

TECH LIBRARY KAFB, NM  
014425

**NACA**

# RESEARCH MEMORANDUM

INVESTIGATIONS AT SUPERSONIC SPEEDS  
OF THE BASE PRESSURE ON BODIES OF REVOLUTION  
WITH AND WITHOUT SWEEPBACK STABILIZING FINS

By Eugene S. Love and Robert M. O'Donnell

Langley Aeronautical Laboratory  
Langley Field, Va.

Classification cancelled: ~~CONFIDENTIAL~~

Authority. NACA Research Abstract No. 97, dtd. 15 Nov. 45

HAAC Technical Library

Civ. Lib. Asst. Jm.

CLASSIFIED DOCUMENT

12 Sept 56

This material contains information affecting the National Defense of the United States within the meaning of the espionage laws, Title 18, U.S.C., Secs. 793 and 794, the transmission or revelation of which in any manner to an unauthorized person is prohibited by law.

**NATIONAL ADVISORY COMMITTEE  
FOR AERONAUTICS**

WASHINGTON  
December 23, 1952

~~CONFIDENTIAL~~

319.18/11



## NATIONAL ADVISORY COMMITTEE FOR AERONAUTICS

## RESEARCH MEMORANDUM

INVESTIGATIONS AT SUPERSONIC SPEEDS  
OF THE BASE PRESSURE ON BODIES OF REVOLUTION  
WITH AND WITHOUT SWEEPBACK STABILIZING FINS

By Eugene S. Love and Robert M. O'Donnell

## SUMMARY

An investigation has been made at Mach numbers of 1.62, 1.93, and 2.41 to determine the base pressure on bodies of revolution with and without sweptback stabilizing fins. The effects of nose shape and base shape were investigated for a body having a cylindrical center section; and the effects of cut-off length were investigated for a slender parabolic body. The effects of sting diameter and disturbances entering the wake were also determined. The over-all Reynolds number range of the tests was approximately from  $1 \times 10^6$  to  $10 \times 10^6$ , based on body length.

The results showed that varying the Reynolds number has little effect upon the base pressure of finned bodies and that the variation of base pressure with Reynolds number for unfinned bodies follows the pattern described in NACA RM L52H21 and the qualitative predictions of Crocco and Lees. The effect of nose shape was small and essentially the same for both the finned and unfinned bodies. Some of the base shapes, though considerably different geometrically, realized approximately the same base pressure because of their similar wakes. For the parabolic body, the variation in base pressure with cut-off length followed closely the trend and magnitude of the pressure on the body surface just ahead of the base. This variation in base pressure held true for the rearmost portion of the body where the pressure recovery created positive pressures. The base pressure of the parabolic body was more sensitive to variations in sting diameter than were the base pressures for the bases of the body with a cylindrical center section. Indications are that disturbances may be permitted closer to the base for sting-supported bodies than for bodies in free-flight condition. For sweptback fins of the type employed in this investigation and similarly located with respect to the base, the effects of the fins upon the base pressure are essentially viscous effects that are, for the most part, eliminated when the Reynolds number for natural transition on the body without fins is exceeded.

## INTRODUCTION

The problem of accurately predicting the base pressure on bodies of revolution at supersonic speeds continues to receive considerable attention in the design of supersonic aircraft and missile bodies. To date, no method has been presented for evaluating base pressure that includes all of the primary influencing variables. Accordingly, an accumulation of experimental data covering various combinations of the variables seems necessary. A number of comprehensive experimental investigations have been conducted along these lines in recent years. Although most of this work has been done in wind tunnels, free-flight investigations have also made significant contributions, particularly in that free-flight results offer comparative data with and without support systems similar to those employed in wind-tunnel work. The support-interference effects on base pressure have probably received as much, if not more, study in wind-tunnel investigations than the primary influencing variables common to actual flight, and this emphasis seems necessary if extrapolations of data to conditions of zero support interference are to be reliable.

The purpose of the present investigation was to obtain additional experimental base-pressure data for bodies of revolution. In this investigation an attempt has been made to duplicate free-flight conditions in the wind tunnel, insofar as base pressure is concerned, for bodies having sweptback cruciform stabilizing fins. In these tests the bodies were supported by the sweptback fins. The effects of nose and base shape were investigated for a body having a cylindrical center section. The nose shapes included a radome contour, an ogive, and a cone; the base shapes were conical, cylindrical, cusp, and abrupt boattail. The effects of varying the base area on a parabolic body were investigated by varying the afterbody length to give base areas from approximately zero to that immediately aft of the fin-body juncture. The effects of sting-support diameter and the effects of disturbances entering the wake in terms of distance from the base were investigated for the representative base configurations. In the tests described above the Reynolds number was varied within a range approximately from  $3 \times 10^6$  to  $8 \times 10^6$ , unless Reynolds number effect had been shown to be insignificant.

For assessing the effects of the fins upon base pressure, the models were tested without fins and mounted on sting supports. In these tests the Reynolds number was varied from approximately  $1 \times 10^6$  to  $10 \times 10^6$ . With minor exceptions, all tests were conducted at Mach numbers of 1.62, 1.93, and 2.41.

## SYMBOLS

M	Mach number
$P_B$	base-pressure coefficient, $\frac{P_B - P_0}{q_0}$
x	distance measured parallel to center line of body
y	distance measured normal to center line of body
R	Reynolds number based on body length
L	actual body length (tip-to-tip for parabolic body)
D	maximum body diameter
h	base diameter
d	sting diameter
b	fin span, normal to center line of body
$\Delta P_B$	fin effect on base pressure, $(P_B)_{\text{with fins}} - (P_B)_{\text{without fins}}$
r	radius
$h_w$	wake diameter
P	pressure coefficient
$P_B$	base pressure
$P_0$	free-stream static pressure
$q_0$	free-stream dynamic pressure

## APPARATUS

## Wind Tunnel

The Langley 9-inch supersonic tunnel is a continuous-operation, closed-circuit type in which the pressure, temperature, and humidity of the enclosed air can be regulated. Different test Mach numbers are

provided by interchangeable nozzle blocks which form test sections approximately 9 inches square. Eleven fine-mesh turbulence-damping screens are installed in the relatively large-area settling chamber ahead of the supersonic nozzle. The turbulence level of the tunnel is considered low, based on the turbulence-level measurements presented in reference 1. A schlieren optical system is provided for qualitative flow observations.

### Models and Supports

A drawing of the model having a cylindrical center section and interchangeable nose and base sections is presented in figure 1. A photograph of these parts is shown in figure 2. The three nose sections were of equal length and consisted of a conical nose of approximately  $10^\circ$  semiapex angle, an ogive nose with a 7.97-caliber radius, and a nose having a radome contour of 1.50-caliber extent. The radome contour was computed from the conditions and relations supplied by the Republic Aviation Corporation that give the limiting shape for a radome which has incidence angles no greater than some specified value ( $70^\circ$  in the present case). The four base sections consisted of a cylindrical base, an abrupt-boattail base, a conical base of approximately  $10^\circ$  slope, and a cusp base defined by the following equation, which gives no discontinuity at the juncture of the cylindrical portion and the base shape and gives zero slope at the rearmost station:

$$r = \frac{6(r_1 - r_2)}{x_2^2} \left( -\frac{x^2}{2} + \frac{x^3}{3x_2} \right) + r_1 \quad (1)$$

In this expression the origin is taken at the intersection of the center line of the body and the perpendicular plane at the end of the cylindrical portion, and the subscripts 1 and 2 denote initial and final conditions, respectively. All the base sections were of equal length and, excluding the cylindrical base section, had equal base areas. The fineness ratio of any combination of nose and base section was 9.167.

A drawing of the parabolic body in position on the fin-supported spindle is shown in figure 3, and a photograph of the model with a breakdown of the removable base segments is shown in figure 4. The shape equation for this body is

$$r = 0.1827x - 0.01854x^2 \quad (2)$$

The tip-to-tip fineness ratio is 10.94; however, it was necessary to cut off a small portion of the base tip to accommodate the access hole for a 0.030-inch base-pressure lead tube. The cut-off was therefore made as shown in figure 3 to an over-all length of 9.75 inches and a minimum base diameter of 0.0376 inches; this made all base segments of equal length (0.50 inch). The fineness ratios represented by the five base segments and the ratios of base diameter to maximum body diameter are tabulated below.

Base	Fineness ratio	$\frac{h}{D}$
A	8.609	0.672
B	9.165	.545
C	9.720	.398
D	10.27	.231
E	10.83	.042

The fineness ratio for base B (9.165) is seen to be essentially the same as that for the body with cylindrical center section (9.167).

Figure 5 presents a drawing of the finned base-pressure mount. The four fins had circular-arc sections and a thickness ratio of approximately 0.08 by actual measurement. At a point believed to be sufficiently far out to have no effect on base pressure, the fin chord was increased as shown for strength. All of the fins were swept back  $45^\circ$  with respect to the center line of the spindle and therefore of the body. In the tunnel installation the fins lay in planes  $45^\circ$  from the planes of the tunnel side walls and their outer ends were attached to the tunnel side walls. The center line of the spindle was coincident with the center line of the tunnel. A pressure lead tube was inlaid along each of the two upper fins and vented to the pressure chamber within the spindle (see fig. 3). The fins were attached and sealed airtight to the spindle with silver solder, which in conjunction with the gasket arrangement at the base of the spindle prevented any effects from possible leakage through the small beeswax fairings employed in the slots at the fin-body junctures.

A photograph of the parabolic model installed on the mount outside the tunnel is shown in figure 6. (During the tests, models and parts were interchanged without removing the mount from the tunnel.) As shown in figure 3, a tube soldered to the hole in the pressure-chamber cap screw passed through each base segment to the base cavity of the particular base segment under investigation, within which it was terminated well ahead of the base exit. As the body was foreshortened the tube was

cut off by the appropriate amount. Although no leakage was experienced from the base-segment junctures, the tube was coated with stopcock grease wherever it passed through a base segment. For base A of the parabolic body and all the bases employed with the cylindrical center section, no tube was necessary and the hole in the pressure-chamber cap screw was the pressure-sensing point.

All model parts and the mount were constructed of steel and highly polished. All dimensions were within 0.001 inch of the specified values and the surface roughness of the fins and models was of the order of 8 root-mean-square microinches. For tests of the models without fins, the fin-slots in the model parts were filled and faired with soft solder.

A sting support of  $\frac{1}{4}$ -inch diameter, embodying the design of the fin-supported spindle at its forward end and extending over 4 body diameters from the base of each configuration, was employed in these tests.

#### Wake-Disturbance Apparatus

For introducing disturbances into the wake, a fork was constructed as shown in figure 7. The tips of the fork prongs produced similar shocks which entered the wake symmetrically. The fork was mounted by its sting support so that the center line of the sting support was coincident with the extended center line of the body and the plane of the fork was parallel to the plane of the tunnel side walls. The mechanism into which the sting support of the fork was inserted could be moved forward and backward, parallel to the center line of the tunnel, during a test and its position was indicated by numerical counters. As shown in figure 7, the width of the fork prongs was  $\frac{1}{2}$  inch. The shocks introduced into the wake were therefore at least  $\frac{1}{2}$  inch wide. To obtain an indication of the effects of a disturbance of lesser extent, the fork prongs were thinned to  $\frac{1}{8}$  inch for tests with one base only.

#### Dummy Stings

Five dummy stings were employed with the fin-supported models. The diameters of these strings were  $\frac{1}{16}$ ,  $\frac{1}{8}$ ,  $\frac{1}{4}$ ,  $\frac{5}{16}$ , and  $\frac{3}{8}$  inch. The traversing mechanism employed in the wake-disturbance tests was used to mount the stings, and porous washers, having diameters corresponding to the internal diameters of the particular bases and attached to the forward end of the stings, insured symmetrical alinement of the stings with respect to the base openings. The downstream face of these washers was approximately 0.1 inch ahead of the end of the body. The distance between the end of any base and the sting mount exceeded 4 body diameters.

## TESTS

All models and combinations were first tested in the fin-supported condition at Reynolds numbers of  $2.91 \times 10^6$ ,  $5.12 \times 10^6$ , and  $8.06 \times 10^6$  to determine how body, base, and nose shape affect the base pressure. Tests were then conducted for representative base configurations and all the base segments of the parabolic body to determine at what point downstream of the base the disturbances entering the wake from the disturbance fork would cease to have any effect upon the base pressure. The effect of sting diameter was investigated next for representative base configurations and base B of the parabolic body. The distribution of base pressure across base A of the parabolic body was then investigated both in the plane of the fins and  $45^\circ$  from the plane. Some configurations were tested with a transition strip approximately 2.50 inches from the nose of the body. All of these tests were conducted at Mach numbers of 1.62, 1.93, and 2.41.

To assess the fin effects upon base pressure, the parabolic body with base A and all of the nose-base combinations of the body with cylindrical center section were tested in the sting-supported condition, without fins, over a Reynolds number range of approximately  $1 \times 10^6$  to  $10 \times 10^6$  at each of the three Mach numbers.

Throughout the tests the dew point was kept sufficiently low to insure negligible effects from condensation. Representative schlieren photographs were taken of most of the tests and schlieren observations were made in all tests.

## PRECISION

All models, both fin- and sting-supported, were maintained within  $\pm 0.1^\circ$  of zero pitch and yaw with reference to the tunnel side walls and center line, respectively. Past measurements of the flow angularity in the tunnel test section have shown negligible deviations. The estimated accuracies of the test variables and the measured pressures are given below.

Mach number, M	$\pm 0.01$
Reynolds number, R	$\pm 0.04 \times 10^6$
Base pressure coefficient, $P_B$	$\pm 0.003$

The indicated location of the disturbance-generating fork was accurate within  $\pm 0.015$  inch.



Because the reflected shocks from the tunnel walls intersected the wake close to the base at  $M = 1.62$ , particularly so for the radome nose, special tests were made to determine if these shocks were affecting the accuracy of the base-pressure measurements. For these tests a short length of a thin-walled tube approximately 5 inches in diameter was mounted just ahead of the fins so as to be aligned with the flow and symmetrically located with respect to the body axis. The leading edge of this tube segment was beveled to a knife-edge on its outer surface only, retaining zero slope on the inner surface. The reflected nose shocks were intercepted by this apparatus and reflected to the tunnel walls again, thereby moving the point at which shocks entered the wake considerably downstream. The results of these tests showed negligible effects for all configurations except the radome nose, for which the base pressure coefficient was found to be greater by approximately 0.078 for all bases in the absence of the "shock reflector." The base pressure coefficients for these configurations have been corrected by this amount.

## RESULTS AND DISCUSSION

In the discussions to follow, the results of the investigation will be presented in the following order:

- (1) Finned body with varying nose and base shape
- (2) Finned parabolic body with varying cut-off length
- (3) Effects of sting-support diameter
- (4) Pressure distribution across base A; parabolic body
- (5) Effect of disturbances entering wake
- (6) Sting-supported bodies without fins
- (7) Fin effects on base pressure.

Finned body with varying nose and base shape.- The results of the base-pressure measurements for the finned body having cylindrical center section are shown in figure 8 for the various combinations of nose and base shapes. At all Reynolds numbers the effect of nose shape upon base pressure is seen to be secondary for all base shapes. Although the different pressure gradients over the forward part of the body caused by the change in nose shape would be expected to have different effects upon transition of the boundary layer and thereby affect the base pressure, these viscous-pressure gradient effects upon base pressure would be small for a finned body since the fin-body juncture triggers

CONFIDENTIAL

turbulence. (This triggering of the boundary layer will be discussed in more detail subsequently.) The effect of nose shape for the finned bodies is, therefore, predominately a result of the difference in the pressure distribution over the body and the difference in the pressure field about the body caused by the different nose shapes.

Figure 9 presents theoretical Kármán-Moore pressure distributions over the body for the conical nose with cylindrical base and for the ogive nose with cylindrical base and conical base. Each curve represents a 30-point calculation. If the viscous and pressure effects of the fins are assumed to be approximately the same for all nose-base combinations, these distributions give some insight into the small effect of nose shape for the finned bodies. Comparison of the distributions for a given Mach number shows that the pressure on the body becomes essentially the same for both nose shapes at  $\frac{x}{L} \approx 0.8$ . Consequently, the effect of nose shape upon the pressures over the different base shapes, and therefore upon base pressure, would be negligible. This conclusion presupposes, of course, that turbulent flow exists ahead of the base as previously implied. Comparison of the distributions over the cylindrical and conical bases in figure 9(b) shows how base shape alters the pressure and Mach number just ahead of the base, and therefore alters the base pressure.

The data of figure 8 show that at a given Reynolds number the base pressures for the boattail and cylindrical bases are of the same magnitude, and the base pressures for the cusp and conical bases are of the same magnitude. Examination of the schlieren photographs of figures 10 to 15 shows that this correlation between base configurations arises from the geometric similarity of the turbulent wakes enshrouding the bases. Figure 8 also shows that the effect of increasing the Reynolds number is, in general, to increase the base pressure. This increase is small in most instances and might be expected since turbulent flow envelops all or almost all of the base at all Reynolds numbers, either because of the triggering effect of the fins or because the Reynolds number is high enough to cause natural transition ahead of the fin-body juncture. The results of tests made with a transition strip 2.50 inches from the nose at  $R = 2.91 \times 10^6$  are in good agreement with the results at  $R = 8.06 \times 10^6$ , for which natural transition occurred well ahead of the fin-body juncture. For natural transition at  $R = 2.91 \times 10^6$ , laminar flow existed over the entire body except for the triggering effects of the fin-body juncture. Figure 16(a) presents schlieren photographs at  $M = 1.93$  for the conical nose with a transition strip in conjunction with the various bases.

The triggering effect of the fin-body juncture on the body having ogive nose and cylindrical base were observed by the liquid-film

method for several Reynolds numbers at a Mach number of 1.93. Sketches of the observed turbulence spread and the behavior with Reynolds number are presented in figure 17. In general, when laminar flow existed ahead of the fin-body juncture the downstream spread of turbulence was similar to that predicted in reference 2 and illustrated by luminescent-lacquer technique in figure 2 of reference 3. At the lowest Reynolds number the spread of turbulence was small, permitting narrow regions of laminar flow to reach the base. Indications of this condition can be seen in some of the schlieren photographs where the continuation of a free laminar wake downstream of the base from the regions of laminar flow ahead of the base is seen to be small or nonexistent. Therefore, even at the lowest Reynolds number an essentially turbulent wake enshrouds the base, and the base pressure would be expected to reach the low values common to turbulent scavenging. With increasing Reynolds number the spread of turbulence becomes greater in the manner shown in figure 17 until the region of initial transition moves ahead of the juncture of the fin leading edge and body surface. In contrast to the turbulence spread on the body, the turbulence spread on the fin roots is not nearly so marked; in fact, the pattern of turbulence remains almost the same until the transition region moves ahead of the fin-body juncture. When this occurs the region of turbulence on the fins is displaced outboard.

Finned parabolic body with varying cut-off length. - The results of the base-pressure measurements for the various cut-off lengths of the parabolic body are shown in figure 18 as a function of Mach number. The effects of Reynolds number differences resulting from different body lengths are secondary to the indicated effects of Mach number and cut-off length, since a turbulent wake enshrouds all bases at all Reynolds numbers, and the effects of the fins in creating turbulence, as well as the occurrence of natural transition, are similar to the conditions previously discussed. The schlieren photographs of figures 19 to 21 show the base phenomena for the different cut-off lengths, Reynolds numbers, and Mach numbers. The spread of turbulence from the fin-body juncture with increasing Reynolds number is indicated clearly in a number of the photographs. Further indications of small Reynolds number effect upon the base pressure is obtained by comparing the results for natural transition with those obtained with a transition strip fixed 2.50 inches from the nose (figs. 18(a) and 18(b)). Schlieren photographs of the parabolic body with fixed transition at  $M = 1.93$  are shown in figure 16(b). Although no data were obtained at  $M = 2.41$  for bases B to D for fixed transition, an extrapolation following the trends for bases A and E would seem reasonable.

The variations with Mach number for the different bases of the parabolic body are, in general, similar to those exhibited by the body with varying nose and base shapes. As the cut-off length of the parabolic body is increased, the Mach number corresponding to maximum base drag increases. This variation also corresponds to a decreasing base

area. The results of figure 8 show such an effect of decreasing the effective base area, that is, from cylindrical or boattail base to cusp or conical base.

Figure 22 presents the effect of cut-off length on the base pressure. The large increase in base pressure with increasing length (decreasing base area) appears to be a result of the variation with cut-off length of the pressure on the body surface immediately ahead of the base. If the viscous and pressure effects of the fins are assumed to be approximately the same for the different bases, the pressure distributions over the body without fins give some insight into the increasing base pressures, which reach positive values for all Mach numbers as the cut-off length approaches body length. The theoretical distributions for the three Mach numbers, given in figure 23, show the rapid pressure recovery over the rear of the body at each Mach number. The portions of these theoretical curves corresponding to the range of values of  $x/L$  for the variation in afterbody length have been entered on figure 22(c) to allow comparison of the variations of the base pressure and the pressure on the surface immediately ahead of the base. (The comparison has been limited to figure 22(c) since the Reynolds number effects are small.) The general agreement in the variations of  $P_B$  and  $P$  with  $x/L$  indicates that the flow about the smaller bases (C, D, and E) is undergoing little, if any, expansion and that the wake boundary is effectively a continuation of the convergent body shape. The schlieren photographs of figures 19 to 21 show that this condition exists for these bases. The base pressure might, therefore, be expected to be in reasonable agreement with the theoretical surface pressures, excluding, of course, values of  $x/L$  very close to 1 where viscous effects severely alter the boundary conditions. The foregoing results would appear to imply that the pressure field created by the fins has little effect on the base pressure for these bases.

Effects of sting-support diameter.— In view of the similarity between the results of figure 8 for the boattail and cylindrical bases and for the cusp and conical bases, the investigation of the effects of sting-support diameter were confined to the boattail and cusp bases. The results for these two bases and base B of the parabolic body are presented in figure 24. Within the range of  $d/h$  values of this investigation the effects of sting-support diameter upon the base pressure of these base configurations (with fins) was small, especially so for the cusp and boattail bases. Mach number does not appear to have any important bearing on the effect of sting-support diameter. For base B of the parabolic body, Reynolds number is seen to have negligible effect, undoubtedly because the wake is turbulent for all values of Reynolds number equal to or greater than the lowest Reynolds number of this investigation. Base B of the parabolic body does appear, however, to be more sensitive to increase in  $d/h$  than the other bases, and for small errors in base pressure measurements a lower limiting value of  $d/h$

would seem desirable. Figure 25, which presents schlieren photographs of the base phenomena for base B of the parabolic body as  $d/h$  is varied, shows that increasing the sting diameter causes the trailing shock to move toward the base. The proximity of this shock to the base for the larger stings might be expected to cause higher base pressures since the pressure rise through the shock might bleed forward in the wake and boundary layer. However, the decreasing base pressure with increasing  $d/h$  shown in figure 24(a) indicates that any such pressure effects from trailing shock are more than overcome by the effects of increasing  $d/h$ , which cause that portion of the annular base area subjected to the highest viscous scavenging (close to the rim of the base) to be a greater percentage of the over-all base area.

Comparison of these results for finned bodies with those of references 4 and 5 for unfinned bodies having turbulent boundary layers ahead of the base indicates that for similar configurations the body with fins does not experience quite as large effects from increasing  $d/h$  as the body without fins.

Pressure distribution across base A; parabolic body.- The results of pressure-distribution measurements across base A of the parabolic body are presented in figure 26. There is apparently no difference between the distribution in line with the plane of the fins and that at a  $45^\circ$  angle to the fin plane. The slightly higher pressure near the center of the base resulting from the circulation within the wake is also evident. Similar results were obtained in the free-flight tests of an ogive-cylinder with circular-arc fins normal to the body axis, reported in reference 6.

Effect of disturbances entering wake.- Figure 27 presents the results of the investigation to determine at what point, downstream of the base, disturbances entering the wake would cease to have any effect upon the base pressure. The position of the disturbance simulator is shown in terms of  $x/D$ , referenced as shown in the sketch at the top of the figure.

At  $\frac{x}{D} = 0$  the shocks from the fork prongs were just touching the lips of the base. This condition and the phenomena for other locations of the disturbance simulator are shown in the schlieren photographs of figure 28 for the configuration with ogive nose and cusp base, with both the large and the small disturbance simulator.

For the bases of the parabolic body, increasing the length, and therefore decreasing the base area, moves the initial point of zero effect from the disturbances closer to the base. Also, the effect of Reynolds number on the location of this point with respect to base B is small. This initial point of zero effect is very likely the point at which all or nearly all of the wake becomes supersonic through induction effects of

the outer stream. As shown by the results for the configuration with ogive nose and cusp base, the weaker shock produced by the small disturbance simulator (see fig. 28) has a relatively small effect on the base pressure, and the initial point of zero effect occurs closer to the base. Disturbances having strengths approaching that of weak shocks or Mach waves might, therefore, be expected to have negligible effects on the base pressure. Examination of the results of figure 27 shows that at a value of  $x/D$  corresponding to that where the reflected nose shock from the radome nose at  $M = 1.62$  intersected the wake ( $\frac{x}{D} \approx 0.2$ ), the large disturbance simulator created pressure rises considerably in excess of that created by the reflected nose shock, which as stated previously was 0.078. Consequently, the present results should give a conservative estimate of the point downstream of the base where reflected shocks and the like may be permitted to enter the wake without affecting the base pressure.

The initial points of zero effect from figure 27 are presented in figure 29 as a function of the ratio of base diameter to body diameter and the ratio of wake diameter to body diameter. The wake diameters used to obtain the latter ratios were obtained from enlargements of schlieren photographs and correspond to conditions exactly at the body base. The wake measurements for the parabolic body are presented in figure 30 as a function of base location. Distinct inner and outer wakes were noted for the more rearward bases (see figs. 19 to 21); these wakes tended to unite into one distinct boundary for the more forward bases. The discrepancies between the values for the most forward base are probably an indication of the accuracy of the measurements, since the inner and outer wakes were measured by different observers. Nevertheless, there is a clear indication that the inner wake follows the body boundary rather closely while the outer wake tends to break away from the body contour near  $\frac{x}{L} = 0.86$ . Examination of the schlieren photographs of figures 19 to 21 shows that the flow is supersonic at least to a boundary that is approximated by the inner wake.

With reference to figure 29 again, the correlation of the wake-diameter measurements with the initial point of zero effect from outside disturbances shows that the inner-wake measurements for the parabolic body are the values to be considered, since the outer-wake measurements do not tend to extrapolate to  $\frac{x}{D} = 0$  for  $\frac{h_w}{D} = 0$ , a necessary condition if the initial point of zero effect corresponds to the initial point of an entirely supersonic wake. Both figures 29(a) and 29(b) show that increasing the Mach number is beneficial in that it moves the initial point of zero effect closer to the base, probably as a result of increased induction effects. Comparison of the results for the configuration with ogive nose and boattail base in both figures 29(a) and 29(b) with the

results for configurations having the same base diameter shows the necessity for considering the viscous effects and assuming a reasonable wake diameter if a reliable estimate of the minimum value of  $x/D$  for zero effect is desired for a given base configuration. Base diameter alone is not a sufficient condition for this estimation.

All of the foregoing results apply, of course, to the finned bodies without sting supports. In reference 4 a similar investigation was made at  $M = 1.53$  for an unfinned sting-supported body with a slight amount of boattailing. Simulated reflected shocks were allowed to enter the wake and the effect upon base pressure was observed. For the turbulent condition of the wake these results, when compared with the results of the present investigation, indicate that the presence of a sting support may permit disturbances to enter the wake closer to the base without affecting the base pressure (provided, of course, the sting diameter has no effect in the absence of disturbances). This favorable effect of the sting's presence with regard to disturbances entering the wake seems to arise from the fact that the sting replaces a large portion of the subsonic core of the wake. Thus, it is possible that a disturbance which affects the base pressure considerably in the absence of a sting support may have little or no effect when the sting support is used if the point at which the disturbance would enter the natural wake in the sting's absence is downstream of the point where the sting diameter exceeds the natural wake diameter.

Sting-supported bodies without fins.— The results of the base pressure measurements for the sting-supported bodies without fins are presented in figures 31 to 34 as a function of Reynolds number. For these results the Reynolds number indicated for a particular variation in the curves may be slightly low (of the order of  $1 \times 10^6$ ) since the filling and fairing of the fin slots and the rounding of the shoulders of the base sections from continual interchange was observed to cause turbulence bursts or premature and asymmetrical transition on some of the configurations as the Reynolds number for transition was approached. An example of premature and asymmetrical transition is shown in figure 35. Except for these effects, the results may be considered reliable.

Figure 36 presents a sequence of schlieren photographs showing the variation of the base phenomena with Reynolds number at  $M = 1.93$  for the body having ogive nose and cusp base. The phenomena are, in general, much the same as observed in reference 1 for a slender parabolic body. At the lower Reynolds numbers the laminar flow separates and trails downstream in a laminar wake until its deflection by the sting support establishes the location of the trailing shock. As shown, the separation masks the contour effects of the base. With increasing Reynolds number, wake transition begins to take place and the point of transition within the wake starts to move toward the base. Accordingly there is increased scavenging of the base area, which in turn permits a greater expansion of

the flow about the base, whereby the base pressure is lowered and the trailing shock is moved toward the base. As the separation ahead of the base is reduced and eliminated by increasing Reynolds number, the base contour begins to have more effect on the phenomena; in the present case a shock originates from the turning of the flow created by the reversed slope at the rear of the cusp base. Here, as in reference 1, when the wake becomes fully turbulent the trailing shock ceases to have any noticeable movement and appears to reach its most forward position as a result of the high turbulent scavenging and the greater expansion of the flow just rearward of the base. The fact that the boundary-layer displacement thickness exactly at the base reaches a minimum just prior to transition on the body surface ahead of the base also favors the forward position of the shock. All of these factors combine to cause the base pressure to reach a minimum just prior to transition on the body surface ahead of the base. With increase in Reynolds number beyond that for initial transition on the body surface ahead of the base, the boundary-layer displacement thickness and the diameter of the turbulent wake increase. The result is that, although the position of the trailing shock remains essentially the same, as does the expansion of the flow rearward of the base, the turbulent scavenging is effectively reduced and the base pressure would be expected to increase.

The association between the observed phenomena and the measured variation in base pressure for the other configurations, as affected by Reynolds number, was much the same as for the configuration with ogive nose and cusp base, subject, of course, to the slight variations introduced in the form of shocks or expansions by the different shapes as the Reynolds number was reached for elimination of separation. The well-defined peaks shown by some of the curves of figures 31 to 34 just prior to the Reynolds number for initial transition on the body may be attributed to the relative variations of the momentum thickness and displacement thickness, as explained in reference 1, as transition is approached.

For the body having varying nose and base shapes, the base pressure curves show that the indicated Reynolds number for initial transition on the body, regardless of base shape, varies systematically with nose shape. This variation shows an increase in Reynolds number for transition on the body as the nose changes from cone to radome to ogive, the variation being largest for the cylindrical and boattail bases at all Mach numbers and least for the conical and cusp bases. The difference between the values of Reynolds number for transition for the conical and ogive noses appears to lie in the degree of adverse pressure gradient on the body just rearward of the point where the nose shape joins the cylindrical center section. The adverse gradients begin at the same station for both nose shapes, but, as shown in figure 9, the theoretical gradient for the conical nose is more severe than that for the ogive nose and would be expected, therefore, to cause the boundary layer to become unstable at a lower Reynolds number. Though no theoretical



pressure distribution was calculated for the radome nose, the adverse gradient created just rearward of the juncture of the radome profile and the cylindrical center section might be expected to be of the same order as that for the ogive nose. However, this adverse gradient for the radome nose would occur at a station ahead of that for the ogive nose and, therefore, transition at the base would occur at a Reynolds number lower than that for the ogive nose. As was the case for the finned bodies, there is no significant effect of nose shape upon the base pressure.

Beyond the Reynolds number for which transition first occurs on the body, there is a significant Mach number effect upon the magnitude of the increase in base pressure. This increase (in percent of the minimum base pressure), as well as the rate of increase, is reduced by increasing Mach number as shown in figure 37(a). Apparently, the increased scavenging that accompanies increasing Mach number offsets the effects of a thickening boundary layer and wake to cause this Mach number effect. The results of the investigation of disturbances entering the wake, presented previously, have indicated an increased scavenging from increasing Mach number. Extrapolations of the results of figure 37(a) seem to indicate that the thickening of the boundary layer and wake and the increased scavenging would tend to nullify each other at a Mach number of about 3 and that transition on the body surface would have little effect on the value of base pressure created by the fully turbulent wake, regardless of body or base shape. The validity of this indication is, of course, subject to experimental confirmation. In figure 37(b) the values of minimum base pressure coefficient are shown as a function of Mach number. The effects of the interdependence of body shape and base shape are seen to be appreciable in the Mach number range of these tests, and no ready extrapolation is indicated for all of the curves as was the case for the curves of figure 37(a). There does appear to be a general tendency toward convergence at higher Mach numbers, but this may be no more than that forced upon the variation by the decrease in limiting base pressure with increasing Mach number.

The results of the base pressure measurements for the unfinned parabolic body with base A (fig. 34) show trends similar to those of the results reported in references 1 and 7 for the RM-10 body, which is also parabolic but of higher fineness ratio. For slender parabolic bodies, in general, there is apparently a consistent "step" in the base pressure curve, in the Reynolds number range below that for transition on the body, which corresponds to the occurrence of wake transition.<sup>1</sup>

---

<sup>1</sup>In the editing of the present paper, one of the reviewers called attention to the recent work of Crocco and Lees (see ref. 8). With minor exceptions, the theoretical predictions of the qualitative effect of Reynolds number upon base pressure made by Crocco and Lees are in agreement with the conclusions of reference 1, which were based entirely on experimental results that included measurement and observation of such phenomena as wake transition.

Fin effects on base pressure.— The effects of the fins on the base pressure are shown in figures 38 and 39, where  $\Delta P_B$  is equal to  $P_B$  with fins minus  $P_B$  without fins. In most instances the effects of the fins for the body with the various nose-base combinations are small (fig. 38). The significant effects appear to be viscous effects from the triggering of the boundary layer by the fin-body juncture when the flow over the body would otherwise be laminar. When the flow over the body is turbulent without the fins, addition of the fins has little effect, as shown by the results at  $R = 8.06 \times 10^6$ . The large fin effects would, therefore, be expected to occur at the lower Reynolds numbers and lower Mach numbers. For the parabolic body with base A (fig. 39) the effects of the fins are particularly large at the lower Reynolds numbers and tend to approach zero as the Reynolds number is approached for which natural transition would occur on the body without fins. Thus, for fins of the type employed in these tests and similarly located with respect to the base, the fin effects upon the base pressure are predominantly viscous effects, regardless of the base or body shape investigated.

A fair approximation of the ratio of fin span to body diameter  $b/D$  that corresponds to the fin effects described in the preceding paragraph may be calculated from the measured initial point downstream of the base where strong disturbances entering the wake were found to have no effect, and from the assumption that the fictitious fin tip produces a disturbance inclined at a Mach angle corresponding to the free-stream Mach number. The intersection of the Mach line passing through the initial no-effect wake point with the leading edge of the fin would thus determine the fin span. The values of  $b/D$  calculated on this basis are presented in figure 40. Values greater than those shown would have the same fin effects, since the tip disturbances would enter the wake downstream of the initial no-effect point. Values somewhat less than those shown should cause little variation in the fin effects, since the fin effects have been shown to be predominantly viscous effects. In addition, the tip disturbances would probably not be as strong as those produced by the thinnest fork used in the disturbance investigation, the effects of which were small and for which the initial no-effect point was closer to the base. All of the fin effects presented previously correspond to that portion of the fins which is circular arc in section, since all

values of  $b/D$  shown in figure 40 are well below the value of  $\frac{b}{D} = 6.9$  that defines the point on the fins where the fin section ceases to be a circular arc.

## CONCLUSIONS

An investigation has been made at Mach numbers of 1.62, 1.93, and 2.41 of the base pressure on bodies of revolution with and without swept-back stabilizing fins. The effects of nose shape and base shape were investigated for a body having a cylindrical center section, and the effects of cut-off length were investigated for a slender parabolic body. The effects of sting diameter and disturbances entering the wake were also determined. The over-all Reynolds number range of the tests was approximately from  $1 \times 10^6$  to  $10 \times 10^6$ , based on body length. The following conclusions were indicated:

1. For finned bodies, the effect of varying Reynolds number is small since, except for very low Reynolds numbers, the fin-body juncture creates a turbulent boundary layer that completely enshrouds the base.

2. The variation of base pressure with Reynolds number for all the unfinned bodies of these tests followed the pattern described in NACA RM L52H21 and also in the theoretical results of Crocco and Lees. This variation appears to be typical for bodies of revolution in general.

3. For unfinned bodies, indications are that beyond a Mach number of approximately 3, transition on the body surface would have little effect on the value of base pressure created by a fully turbulent wake, regardless of base shape or body shape.

4. The effect of nose shape was small for both the finned and unfinned bodies. The only significant effects for the unfinned bodies were the small changes in the Reynolds number of transition, which varied according to the severity of the adverse pressure gradient just rearward of the juncture of the nose with the cylindrical center section of the body. The "triggering" of the boundary layer at the fin-body juncture eliminated this viscous-pressure-gradient effect for the finned bodies.

5. Some of the base shapes, though considerably different geometrically, produced approximately the same base pressure because of their similar wakes. This result was true for both the finned and unfinned bodies.

6. For the parabolic body, the variation in base pressure with cut-off length followed closely both the magnitude and trend of the pressure on the body surface immediately ahead of the base. This variation in base pressure held true for the rearmost portion of the body where the pressure recovery created positive pressures.

7. For sweptback fins of the type employed in this investigation and similarly located with respect to the base, the effects of the fins upon the base pressure are essentially viscous effects that result from the creation of a turbulent boundary layer by the fin-body juncture when the flow in the absence of fins would be laminar. Therefore, when the flow ahead of the base is turbulent for the no-fins condition, addition of the fins has only a small effect on base pressure.

8. Varying the diameter of the sting in the presence of the finned bodies had little effect upon the base pressure for the bases of the body having a cylindrical center section. For the finned parabolic body the base pressure was more sensitive to changes in sting diameter.

9. The point downstream of the base of the finned bodies (no sting support) where disturbances entering the wake ceased to affect the base pressure moved closer to the base with increasing Mach number and appeared to be a function of the wake diameter at the base, the Mach number, and the base geometry. Comparisons with results for sting-supported bodies having turbulent boundary layers ahead of the base indicated that disturbances may be permitted closer to the base of the body for sting-supported bodies than for bodies in free-flight condition.

Langley Aeronautical Laboratory,  
National Advisory Committee for Aeronautics,  
Langley Field, Va.

## REFERENCES

1. Love, Eugene S., Coletti, Donald E., and Bromm, August F.: Investigation of the Variation With Reynolds Number of the Base, Wave, and Skin-Friction Drag of a Parabolic Body of Revolution (NACA RM-10) at Mach Numbers of 1.62, 1.93, and 2.41 in the Langley 9-Inch Supersonic Tunnel. NACA RM L52H21, 1952.
2. Loitsianskii, L. G., and Bolshakov, V. P.: On Motion of Fluid in Boundary Layer Near Line of Intersection of Two Planes. NACA TM 1308, 1951.
3. Stalder, Jackson R., and Slack, Ellis G.: The Use of a Luminescent Lacquer for the Visual Indication of Boundary-Layer Transition. NACA TN 2263, 1951.
4. Chapman, Dean R.: An Analysis of Base Pressure at Supersonic Velocities and Comparison With Experiment. NACA Rep. 1051, 1951. (Supersedes NACA TN 2137.)
5. Perkins, Edward W.: Experimental Investigation of the Effects of Support Interference on the Drag of Bodies of Revolution at a Mach Number of 1.5. NACA TN 2292, 1951.
6. Hill, Freeman K., and Alpher, Ralph A.: Base Pressures at Supersonic Velocities. Jour. Aero. Sci., vol. 16, no. 3, Mar. 1949, pp. 153-160.
7. Czarnecki, K. R., and Marte, Jack E.: Skin-Friction Drag and Boundary-Layer Transition on a Parabolic Body of Revolution (NACA RM-10) at a Mach Number of 1.6 in the Langley 4- by 4-Foot Supersonic Pressure Tunnel. NACA RM L52C24, 1952.
8. Crocco, Luigi, and Lees, Lester: A Mixing Theory for the Interaction Between Dissipative Flows and Nearly-Isentropic Streams. Rep. No. 187, Princeton Univ. Aero. Eng. Lab., Jan. 15, 1952.

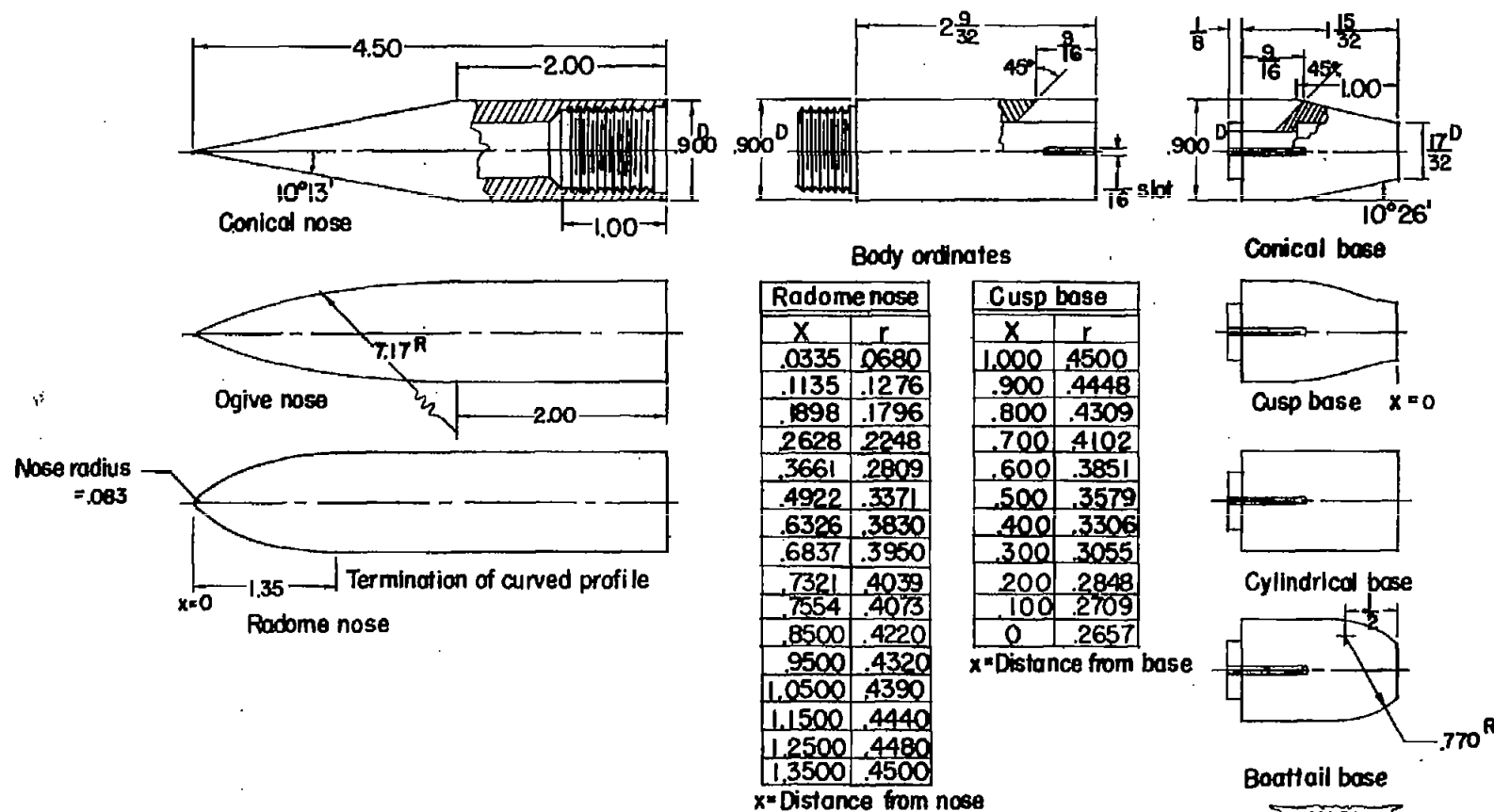


Figure 1.- Drawing of model having variable nose and base sections.  
All linear dimensions are in inches.

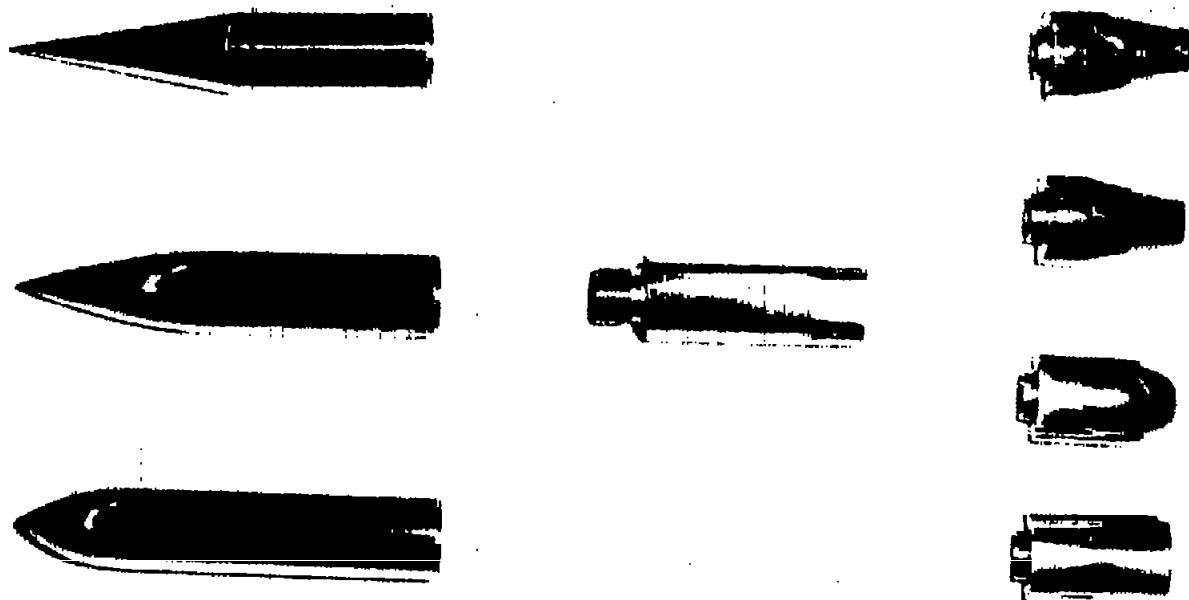


Figure 2.- Photograph of model having variable nose and base sections.

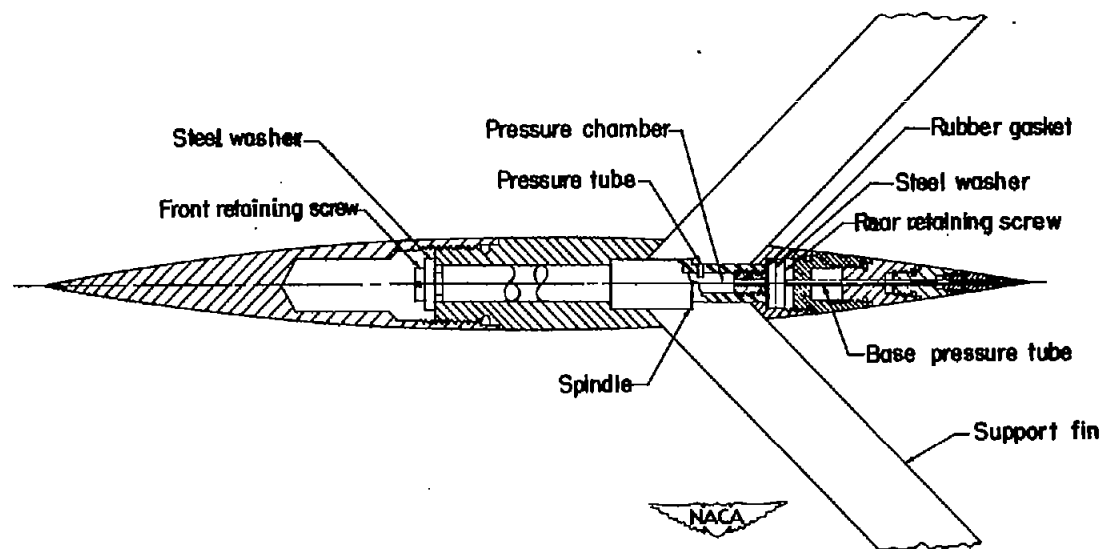


Figure 3.- Drawing of parabolic model and details of installation on fin-supported spindle.

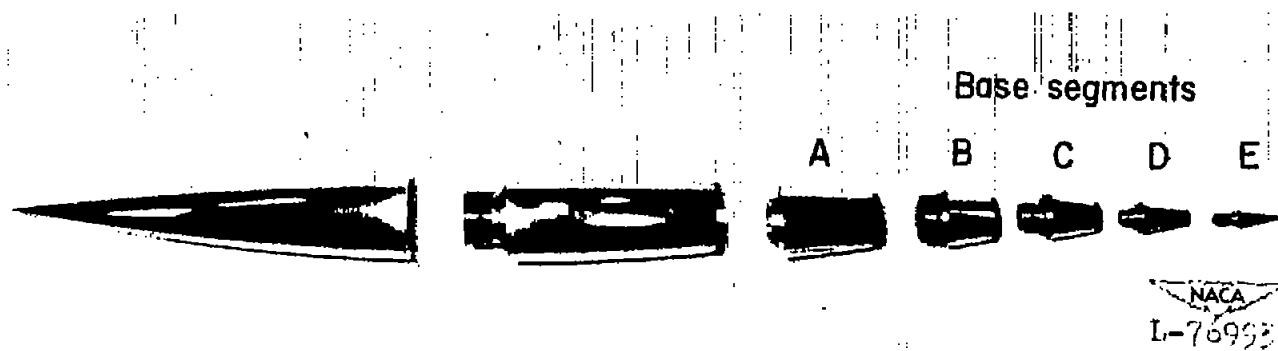


Figure 4.- Photograph of parabolic model.



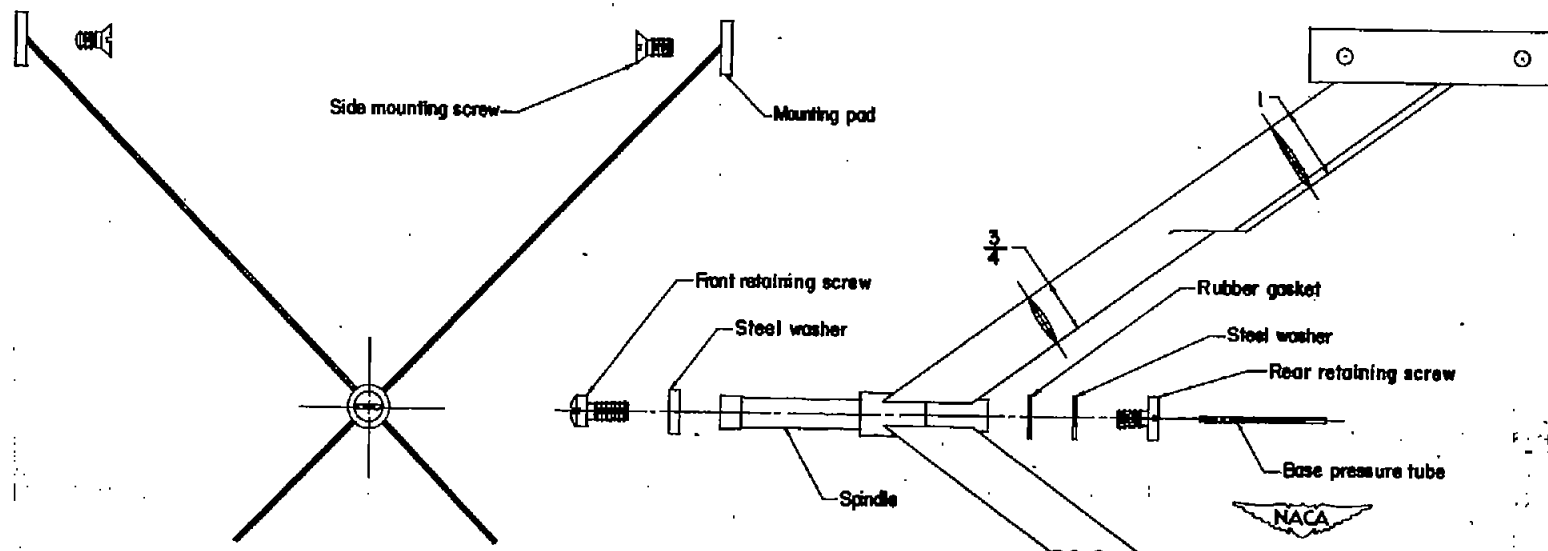
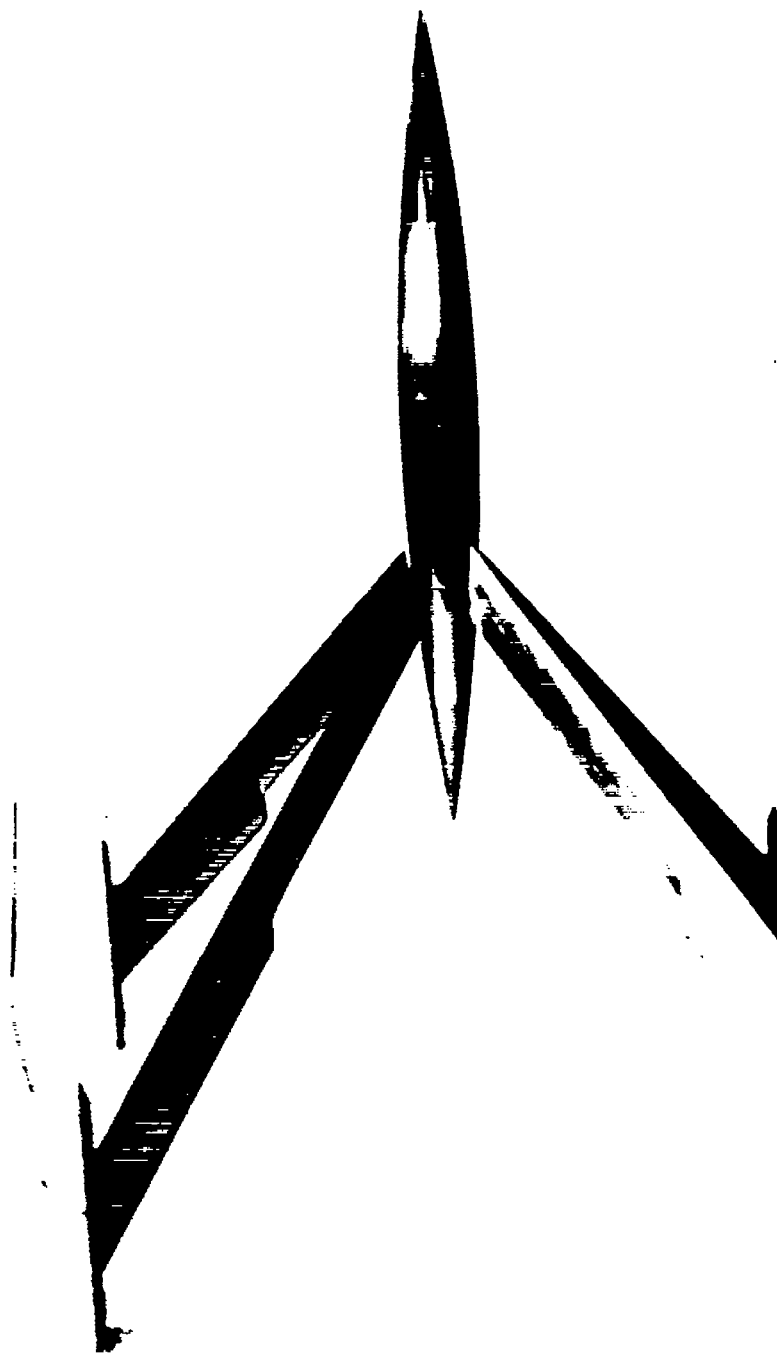


Figure 5.- Details of fin-supported base-pressure spindle. All dimensions are in inches.



NACA

Figure 6.- Photograph of parabolic body on fin-supported spindle.

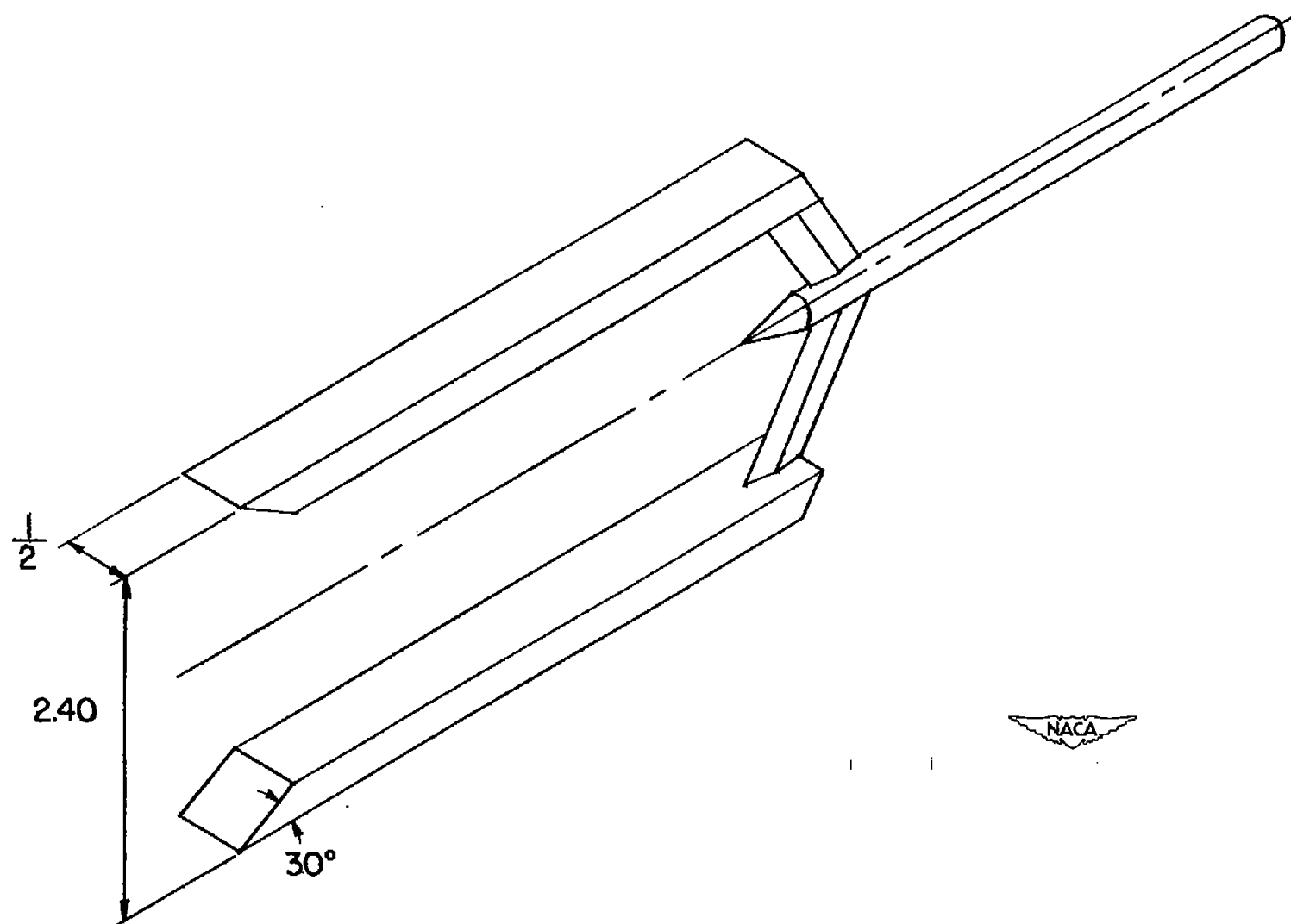


Figure 7.- Disturbance-simulator fork. All linear dimensions are in inches.

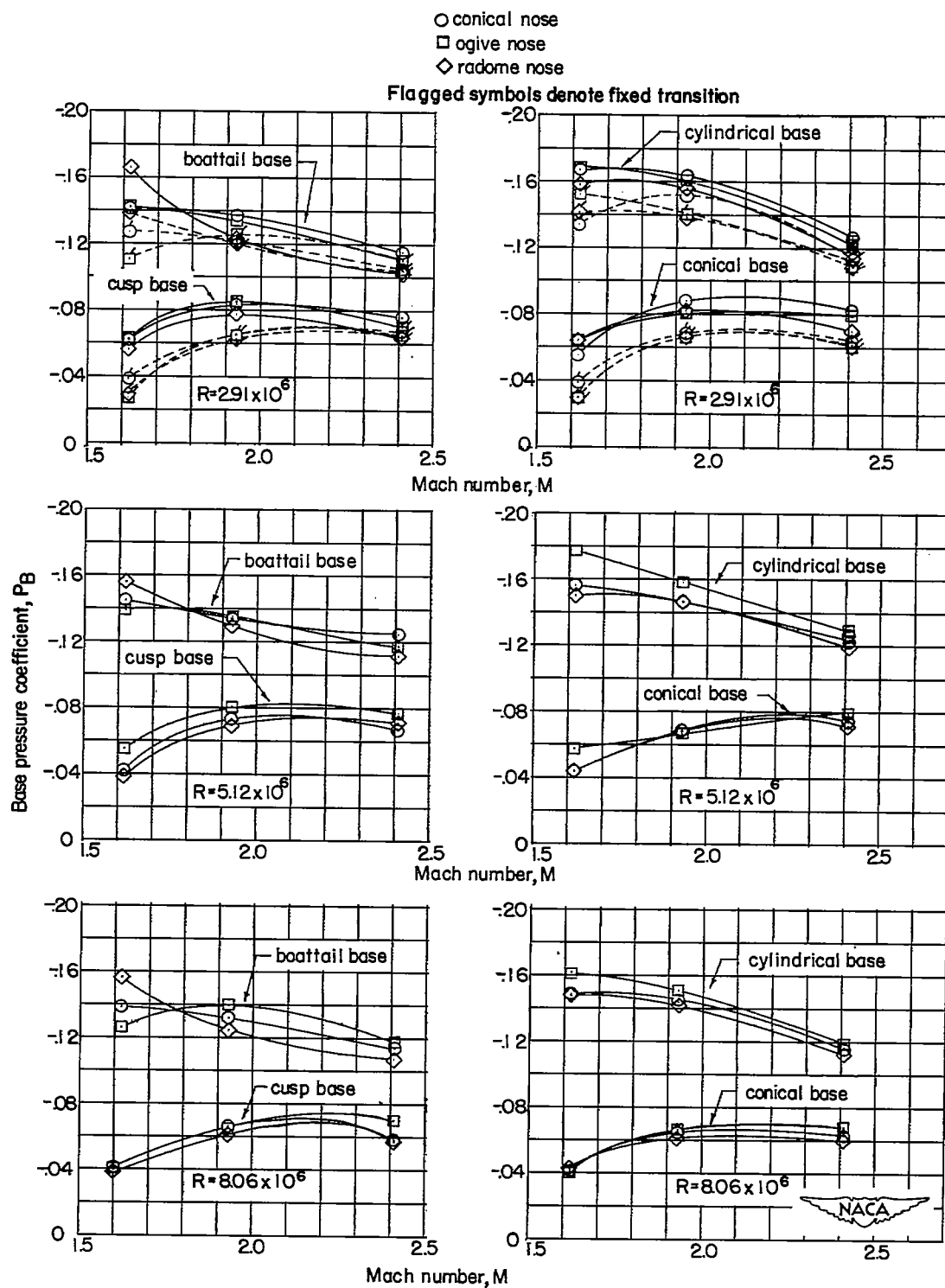
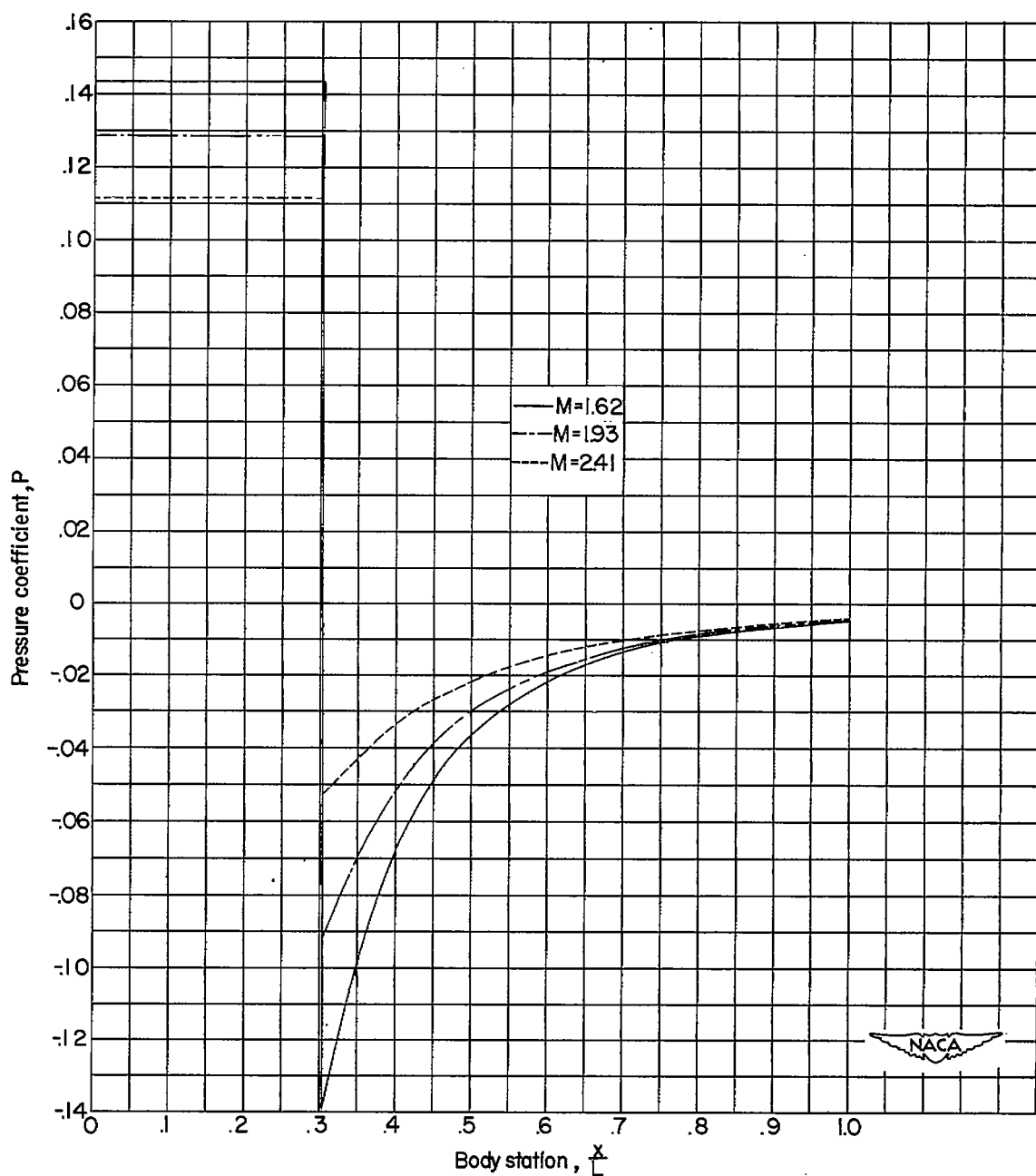
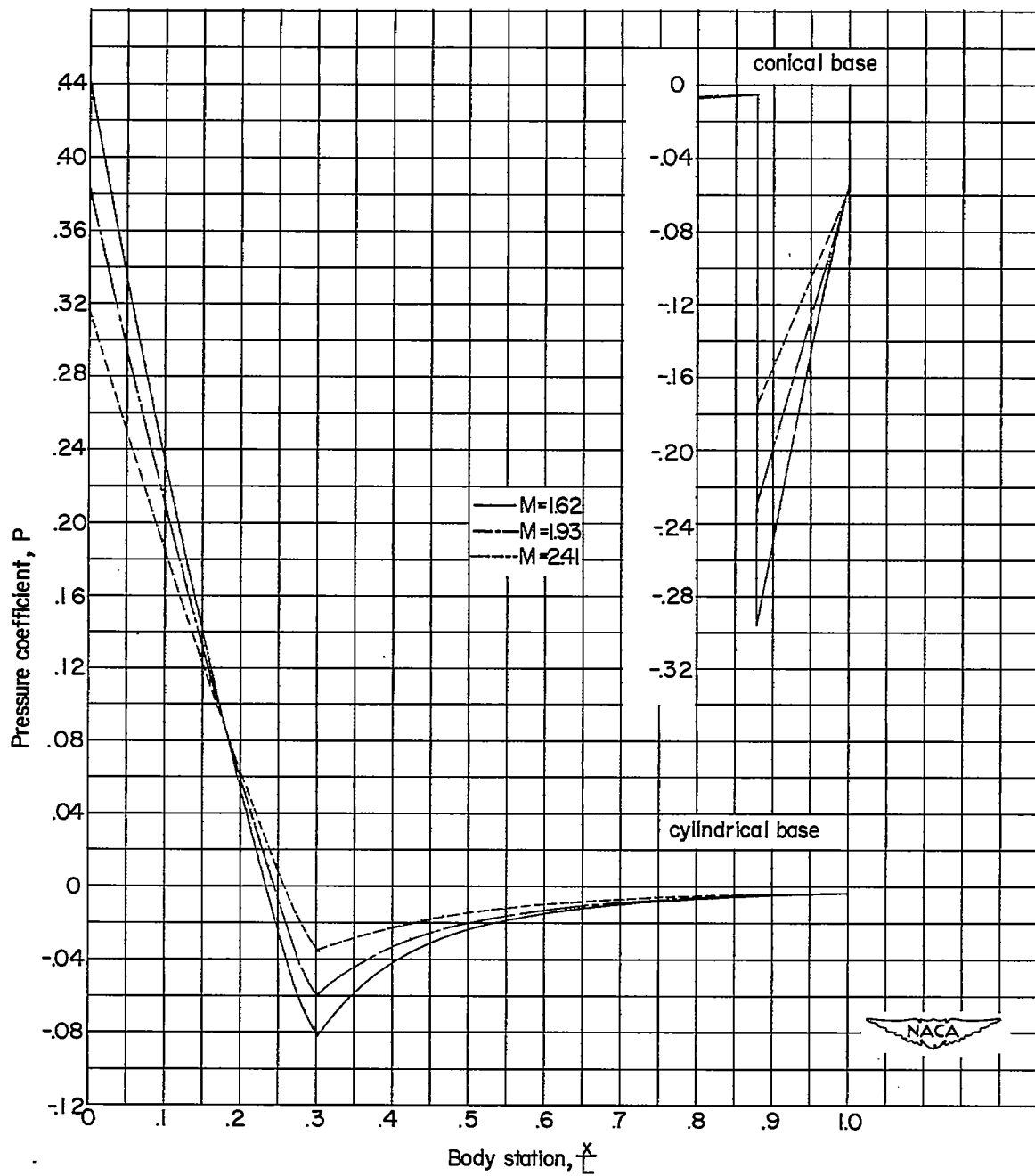


Figure 8.- Effect of Mach number and Reynolds number upon the base pressure of the finned body having variable nose and base shapes.



(a) Conical nose with cylindrical base.

Figure 9.- Theoretical pressure distributions over unfinned body.



(b) Ogive nose with cylindrical and conical bases.

Figure 9.- Concluded.


 $R = 291 \times 10^5$ 
 $R = 5.12 \times 10^6$   
 (a) Boattail base.

 $R = 8.06 \times 10^6$ 

 $R = 291 \times 10^5$ 
 $R = 5.12 \times 10^6$   
 (b) Cylindrical base.


 $R = 8.06 \times 10^6$ 
  
 L-76995

Figure 10.- Schlieren photographs of phenomena at  $M = 1.62$  for the conical nose and the various bases of the finned body.



$R = 2.91 \times 10^6$

$R = 5.12 \times 10^6$   
(c) Cusp base.

$R = 8.06 \times 10^6$



$R = 2.91 \times 10^6$

$R = 5.12 \times 10^6$   
(d) Conical base.

$R = 8.06 \times 10^6$

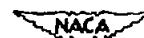


Figure 10.- Concluded. L-76996




 $R = 2.91 \times 10^6$ 
 $R = 5.12 \times 10^6$   
 (a) Conical nose.

 $R = 8.06 \times 10^6$ 

 $R = 2.91 \times 10^6$ 
 $R = 5.12 \times 10^6$   
 (b) Ogive nose.

 $R = 8.06 \times 10^6$ 

 $R = 2.91 \times 10^6$ 
 $R = 5.12 \times 10^6$   
 (c) Radome nose.


 $R = 8.06 \times 10^6$ 
  
 L-76997

Figure 11.- Schlieren photographs of the phenomena at  $M = 1.93$  for the boattail base and the various noses of the finned body.


 $R = 2.91 \times 10^6$ 
 $R = 5.12 \times 10^6$   
 (a) Conical nose.

 $R = 8.06 \times 10^6$ 

 $R = 2.91 \times 10^6$ 
 $R = 5.12 \times 10^6$   
 (b) Ogive nose.

 $R = 8.06 \times 10^6$ 

 $R = 2.91 \times 10^6$ 
 $R = 5.12 \times 10^6$   
 (c) Radome nose.


 $R = 8.06 \times 10^6$ 
  
 L-76998

Figure 12.- Schlieren photographs of the phenomena at  $M = 1.93$  for the cylindrical base and the various noses of the finned body.


 $R = 2.91 \times 10^6$ 
 $R = 5.12 \times 10^6$   
 (a) Conical nose.

 $R = 8.06 \times 10^6$ 

 $R = 2.91 \times 10^6$ 
 $R = 5.12 \times 10^6$   
 (b) Ogive nose.

 $R = 8.06 \times 10^6$ 

 $R = 2.91 \times 10^6$ 
 $R = 5.12 \times 10^6$   
 (c) Radome nose.


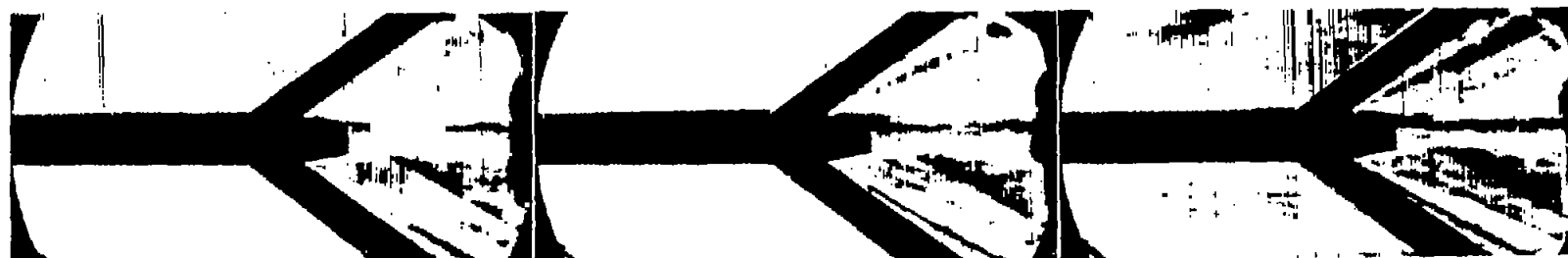
 $R = 8.06 \times 10^6$ 
  
 L-76999

Figure 13.- Schlieren photographs of the phenomena at  $M = 1.93$  for the cusp base and the various noses of the finned body.



$R = 2.91 \times 10^6$

$R = 5.12 \times 10^6$   
(a) Ogive nose.

$R = 8.06 \times 10^6$



$R = 2.91 \times 10^6$

$R = 5.12 \times 10^6$   
(b) Radome nose.

$R = 8.06 \times 10^6$

NACA  
L-77000

Figure 14.- Schlieren photographs of the phenomena at  $M = 1.93$  for the conical base and the ogive and radome noses of the finned body.


 $R = 291 \times 10^6$ 
 $R = 5.12 \times 10^6$   
 (a) Boattail base.

 $R = 8.06 \times 10^6$ 

 $R = 291 \times 10^6$ 
 $R = 5.12 \times 10^6$   
 (b) Cylindrical base.

 $R = 8.06 \times 10^6$ 

 NACA  
 L-77001

Figure 15.- Schlieren photographs of the phenomena at  $M = 2.41$  for the conical nose and the various bases of the finned body.



$$R = 291 \times 10^6$$

$$R = 5.12 \times 10^6$$

(c) Cusp base.

$$R = 8.06 \times 10^6$$



$$R = 2.91 \times 10^6$$

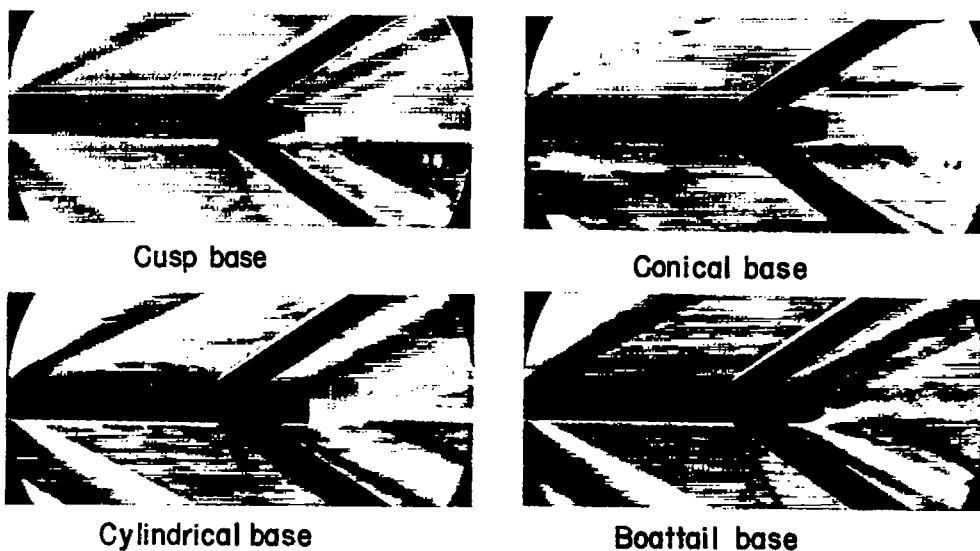
$$R = 5.12 \times 10^6$$

(d) Conical base.

$$R = 8.06 \times 10^6$$

Figure 15.- Concluded. L-77002





(a) Conical nose with various bases.

Base A,  $R=2.74 \times 10^6$ Base B,  $R=2.91 \times 10^6$ Base C,  $R=3.09 \times 10^6$ Base D,  $R=3.26 \times 10^6$ Base E,  $R=3.44 \times 10^6$ 

(b) Parabolic body with varying cut-off length.

NACA  
L-77003

Figure 16.- Schlieren photographs of the phenomena at  $M = 1.93$  with transition strips.

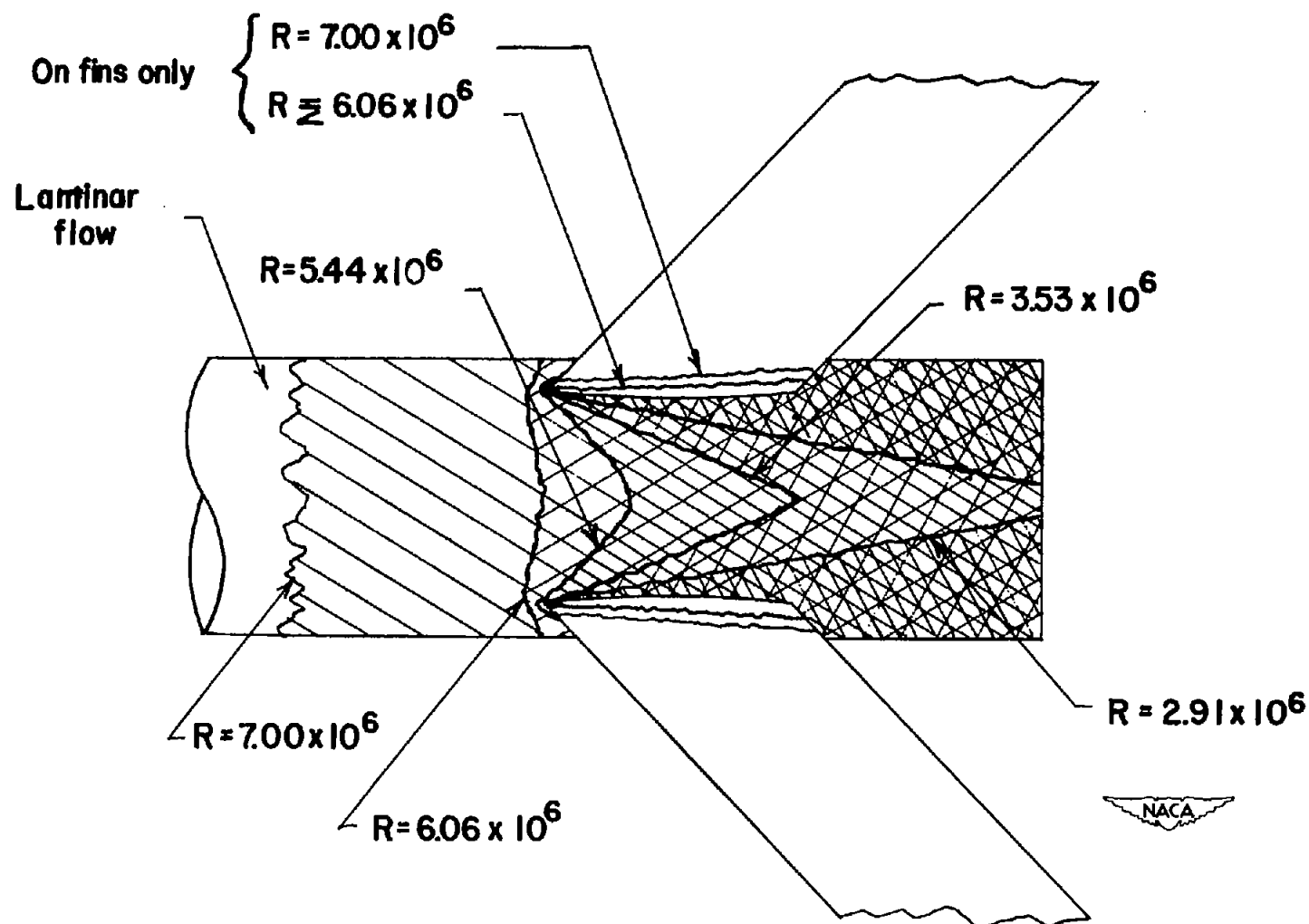


Figure 17.- Limits of turbulent boundary layer with increasing Reynolds number as observed from liquid-film tests at  $M = 1.93$  for model having ogive nose and cylindrical base.



Base	Reynolds number $\times 10^{-6}$		
	○	□	◇
A	2.74	4.82	7.56
B	2.91	5.12	8.06
C	3.09	5.43	8.54
D	3.26	5.74	9.03
E	3.44	6.05	9.52

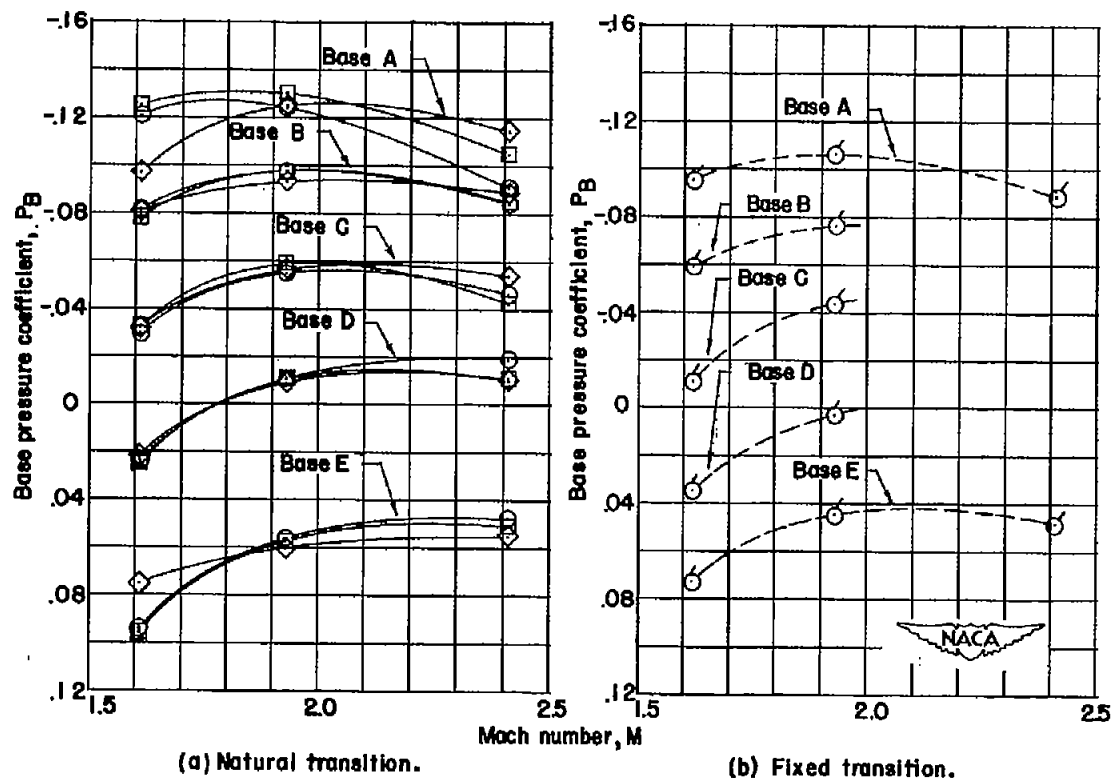


Figure 18.- Effect of Mach number and Reynolds number upon the base pressure of the various bases of the finned parabolic body.



$$R = 2.74 \times 10^6$$

$$R = 4.82 \times 10^6$$

(a) Base A,  $\frac{x}{L} = .795$ .

$$R = 7.56 \times 10^6$$



$$R = 2.91 \times 10^6$$

$$R = 5.12 \times 10^6$$

(b) Base B,  $\frac{x}{L} = .846$ .

$$R = 8.06 \times 10^6$$



$$R = 3.09 \times 10^6$$

$$R = 5.43 \times 10^6$$

(c) Base C,  $\frac{x}{L} = .897$ .

$$R = 8.54 \times 10^6$$

NACA  
L-77004

Figure 19.- Schlieren photographs of the phenomena at  $M = 1.62$  for the various bases of the finned parabolic body.



$$R = 326 \times 10^6$$

$$R = 605 \times 10^6$$

$$R = 9.03 \times 10^6$$

(d) Base D,  $\frac{x}{L} = .949$ .



$$R = 605 \times 10^6$$

$$R = 9.52 \times 10^6$$

(e) Base E,  $\frac{x}{L} = 1.00$ .



Figure 19.- Concluded. L-77005



$R = 274 \times 10^6$

$R = 5.12 \times 10^6$

$R = 7.56 \times 10^6$

(a) Base A,  $\frac{x}{L} = .795$ .



$R = 291 \times 10^6$

$R = 5.12 \times 10^6$

$R = 8.06 \times 10^6$

(b) Base B,  $\frac{x}{L} = .846$ .



$R = 3.09 \times 10^6$

$R = 5.43 \times 10^6$

$R = 8.54 \times 10^6$

(c) Base C,  $\frac{x}{L} = .897$ .



L-77006

Figure 20.- Schlieren photographs of the phenomena at  $M = 1.93$  for the various bases of the finned parabolic body.



$$R = 3.26 \times 10^6$$

$$R = 5.74 \times 10^6$$

$$\text{Base D, } \frac{x}{L} = .949.$$

$$R = 9.03 \times 10^6$$



$$R = 3.44 \times 10^6$$

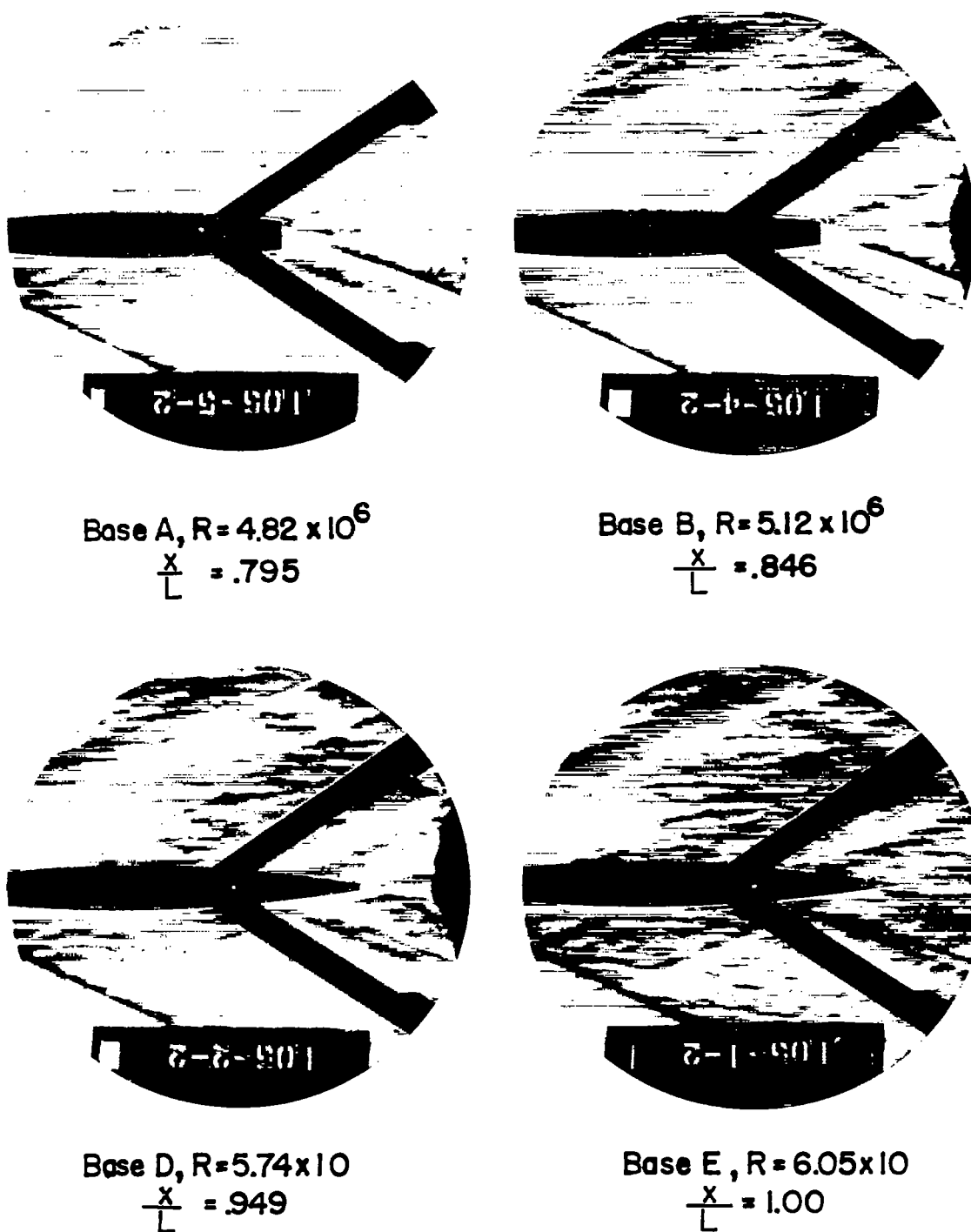
$$R = 6.05 \times 10^6$$

$$\text{Base E, } \frac{x}{L} = 1.00.$$

$$R = 9.52 \times 10^6$$



Figure 20.- Concluded. L-77007



NACA  
L-77008

Figure 21.- Schlieren photographs of the phenomena at  $M = 2.41$  for various bases of the finned parabolic body.

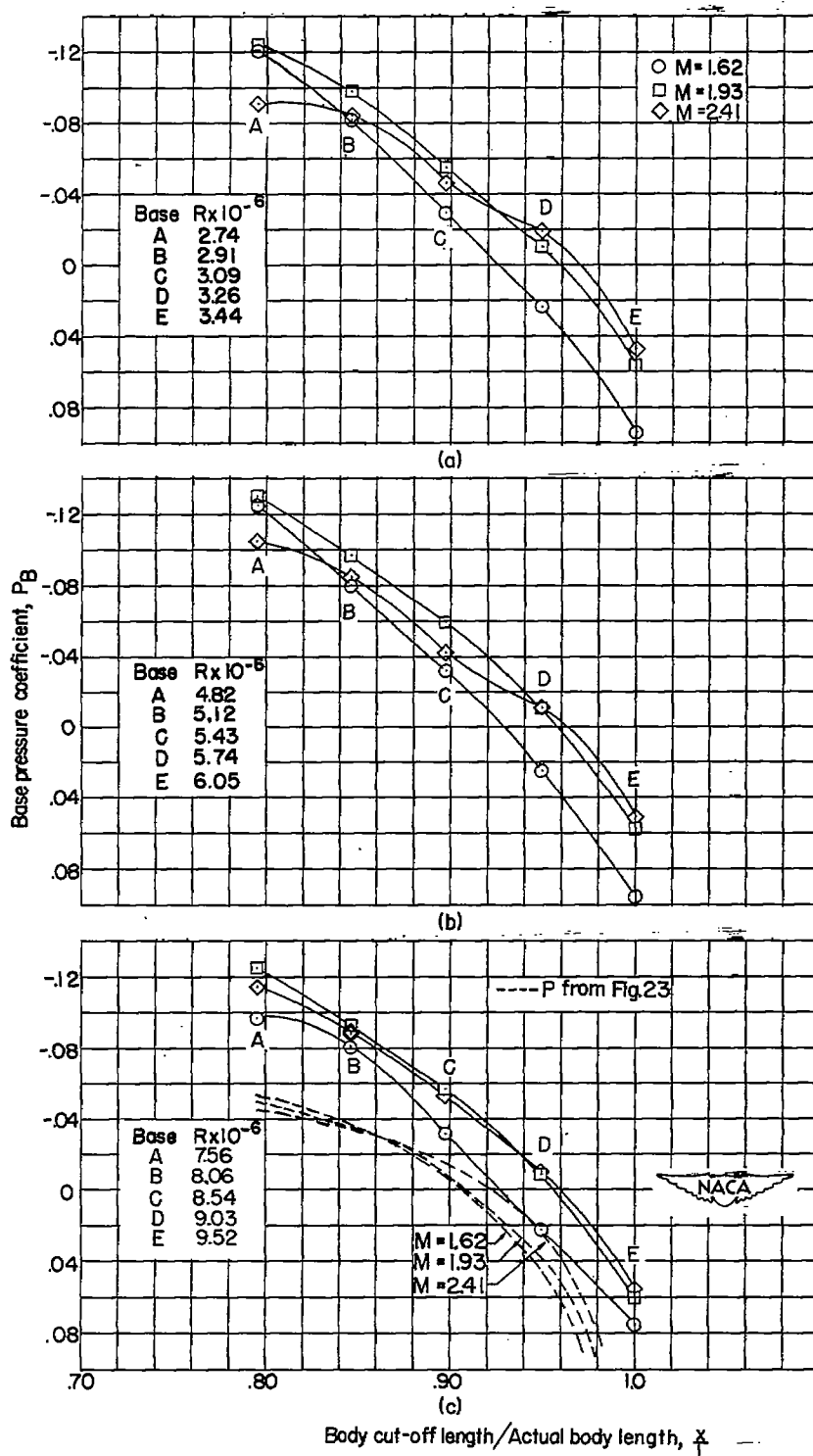


Figure 22.- Effects of cut-off length on the base pressure of the finned parabolic body.

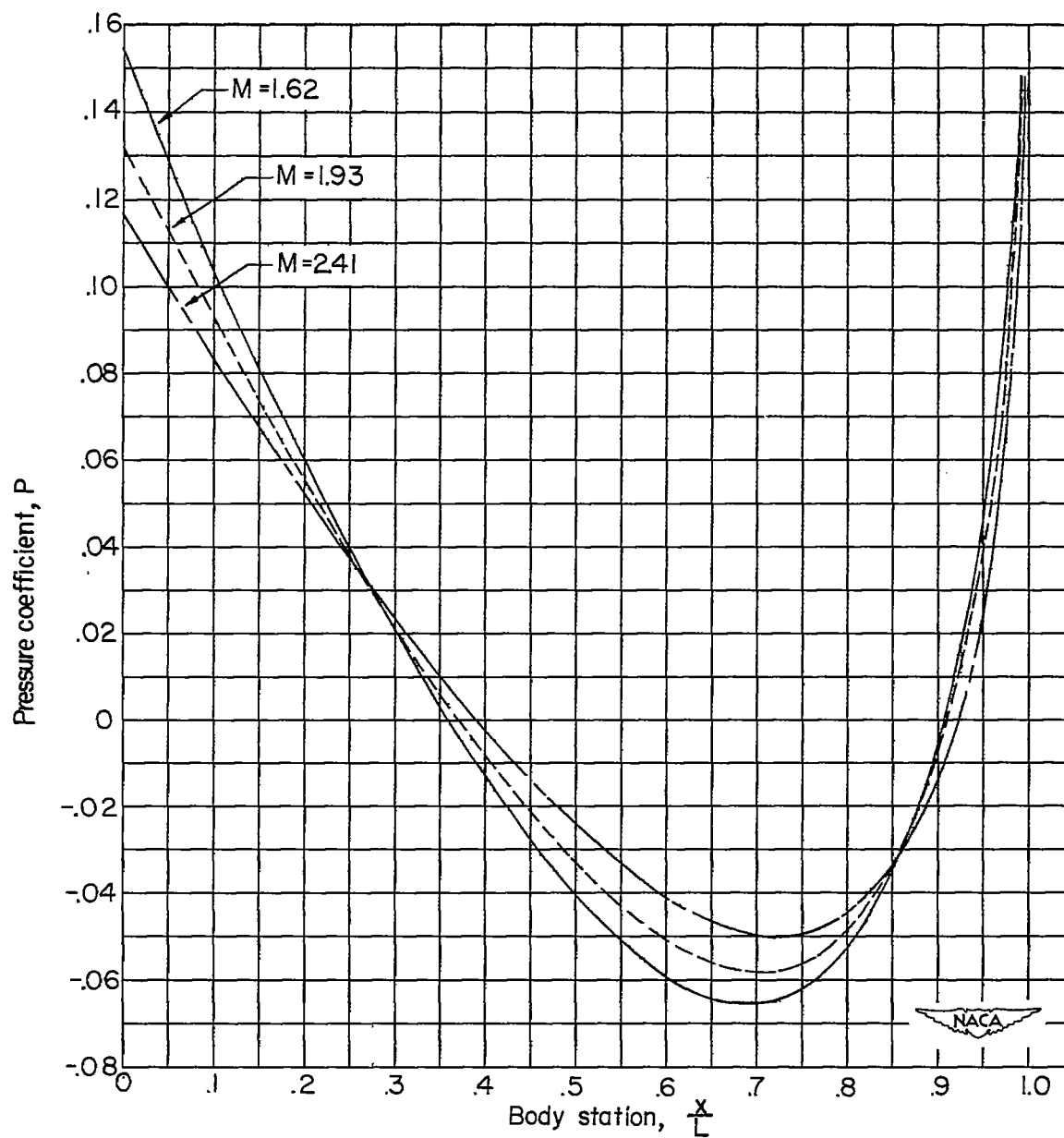


Figure 23.- Theoretical pressure distributions over the unfinned parabolic body.



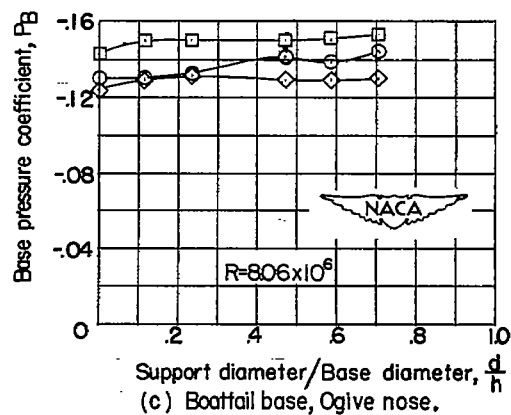
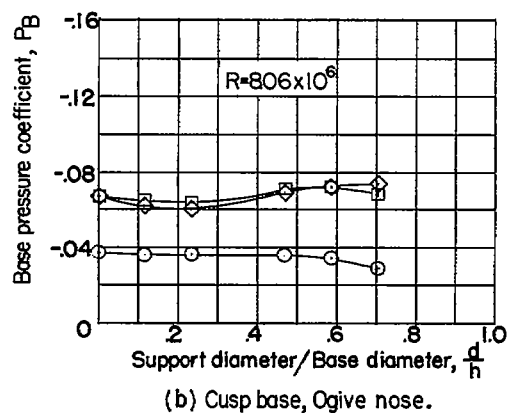
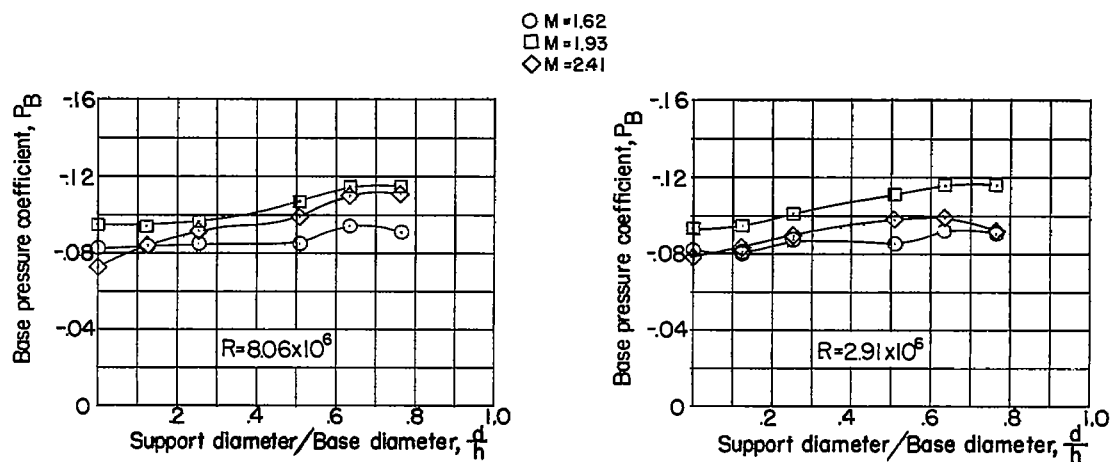


Figure 24.- Effect of sting diameter upon the base pressure of several finned body configurations.

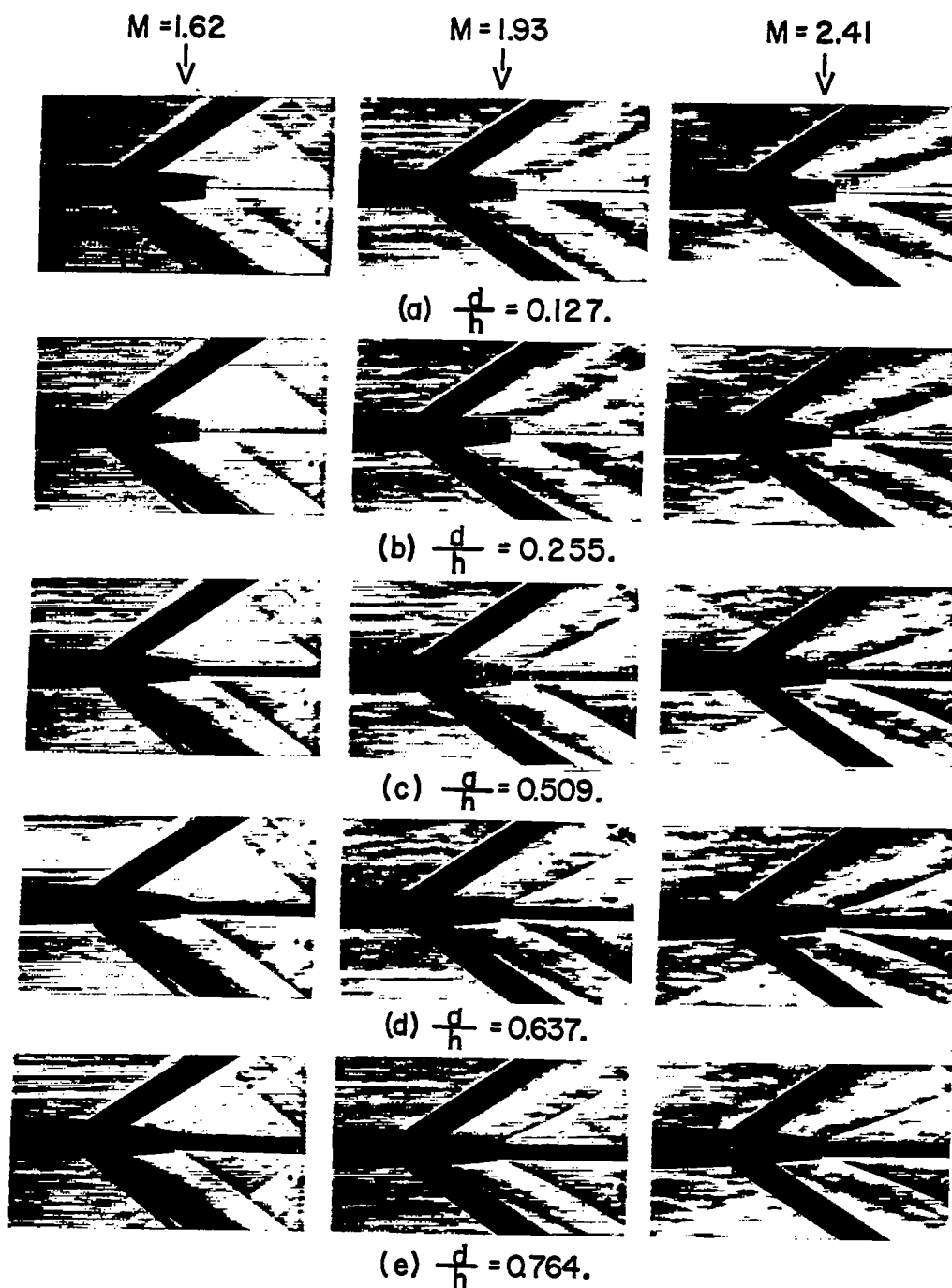

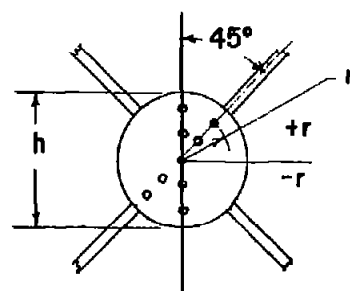


Figure 25.- Schlieren photographs showing the effect of increasing sting diameter upon the base phenomena for base B of the parabolic body at  $R = 2.91 \times 10^6$ .

  
 L-77009



Sketch of orifice locations

- 45° from fin plane
- fin plane

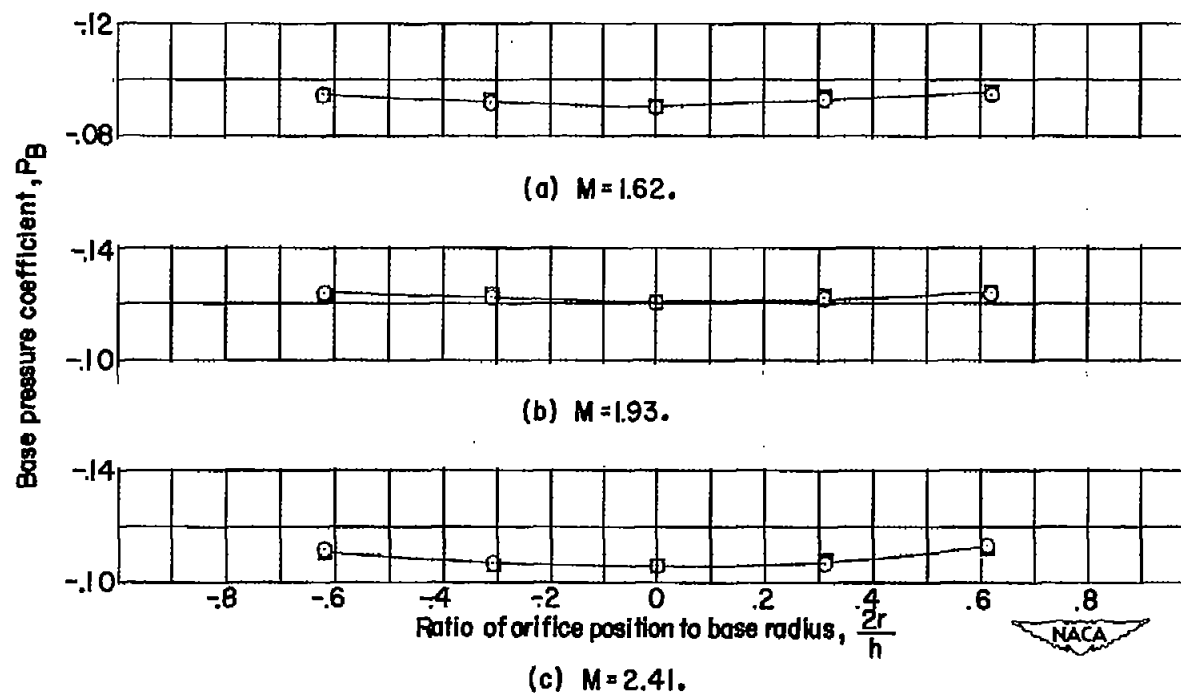


Figure 26.- Distribution of base pressure across base A of the finned parabolic body.

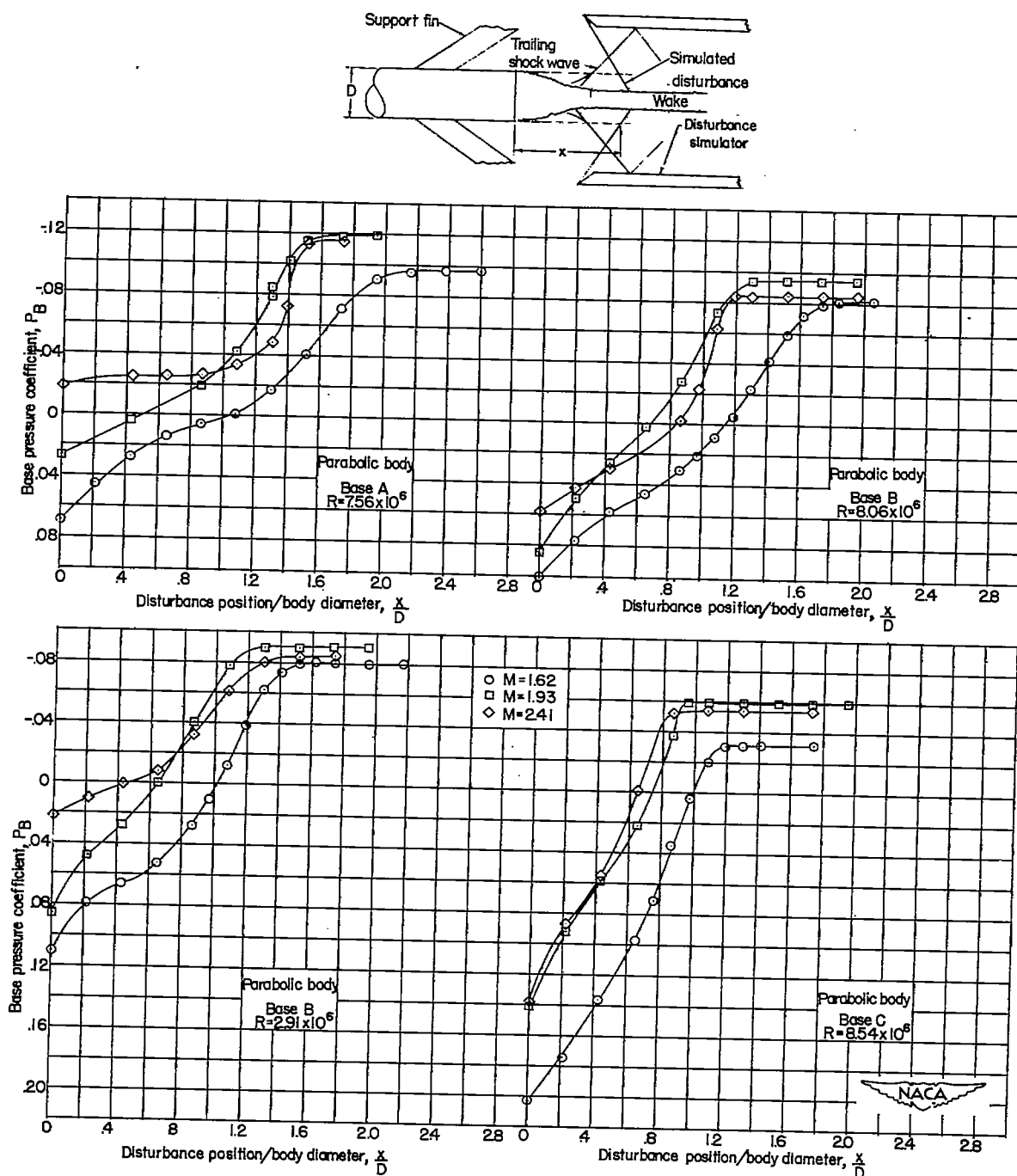


Figure 27.- Effects of disturbances entering the wake upon the base pressure for several finned body configurations (from large disturbance simulator unless otherwise specified).

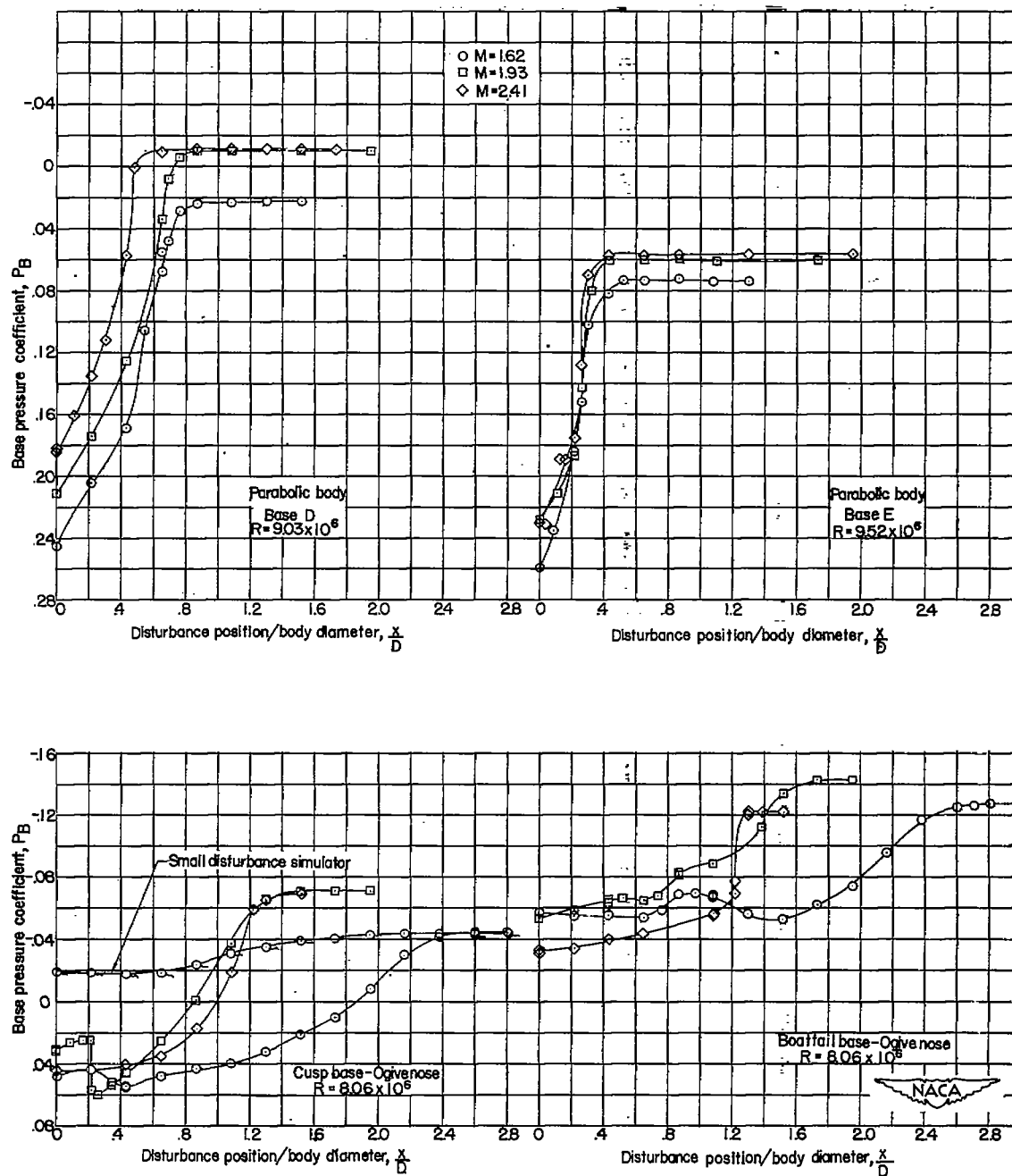


Figure 27.- Concluded.



$$\frac{x}{D} = 0$$



$$\frac{x}{D} = .217$$



$$\frac{x}{D} = .433$$



Large disturbance simulator

Small disturbance simulator

$$\frac{x}{D} = .867$$

NACA  
L-77010

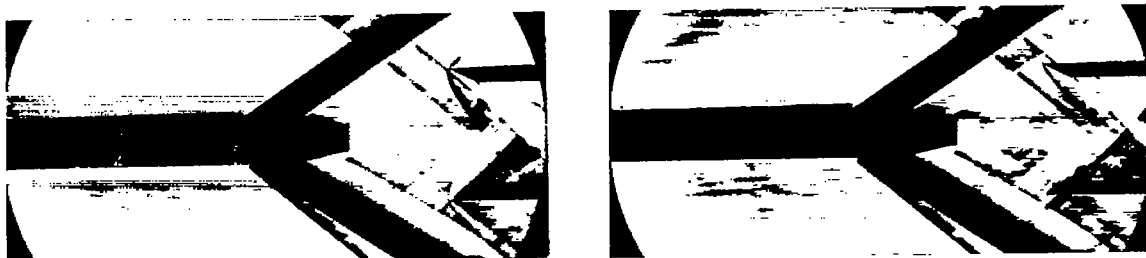
Figure 28.- Schlieren photographs at  $M = 1.62$  of the phenomena associated with the position of the disturbance simulators for the finned body with ogive nose and cusp base.



$$\frac{x}{D} = 1.300$$



$$\frac{x}{D} = 33$$



$$\frac{x}{D} = 2.380$$



Large disturbance simulator  $\frac{x}{D} = 3.031$  Small disturbance simulator



Figure 28.- Concluded.

L-77011

Initial point of zero effect from disturbance simulator,  $\frac{x}{D}$ 

Model	Mach no.		
	1.62	1.93	2.41
Parabolic body	○	□	◇
Ogive nose-Cuspbase	△	▽	◇
Ogive nose-Boattail base	▵	▿	◇

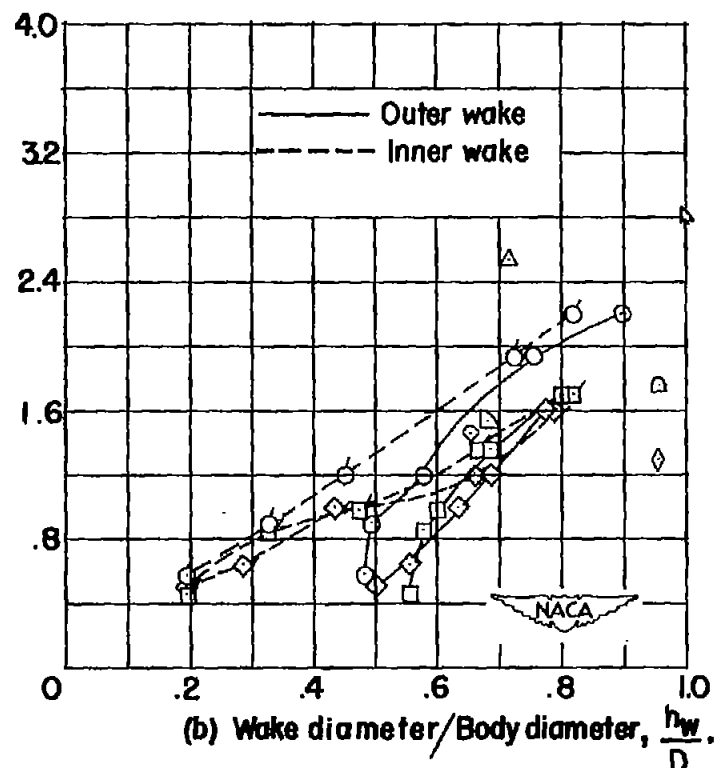
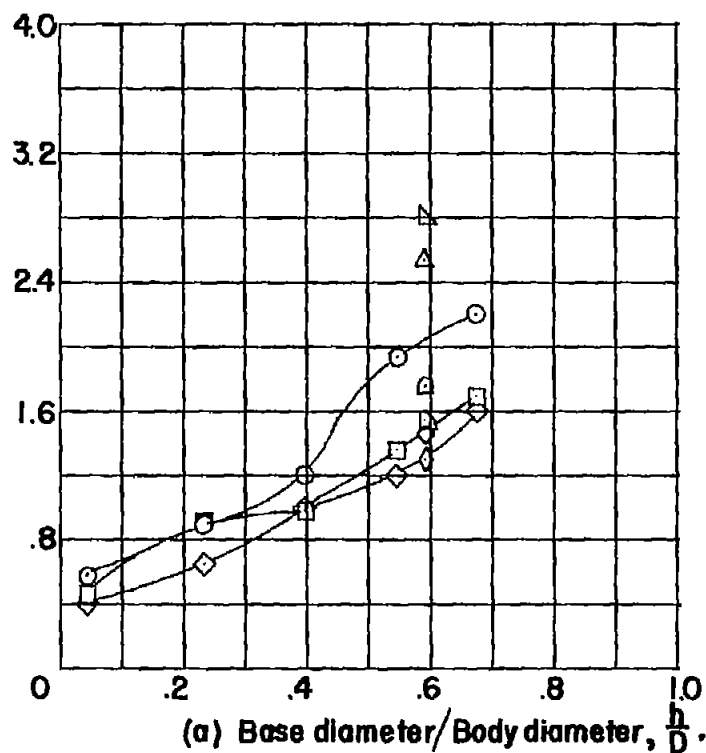


Figure 29.- Initial point of zero effect from disturbance simulator as a function of base diameter and wake diameter.



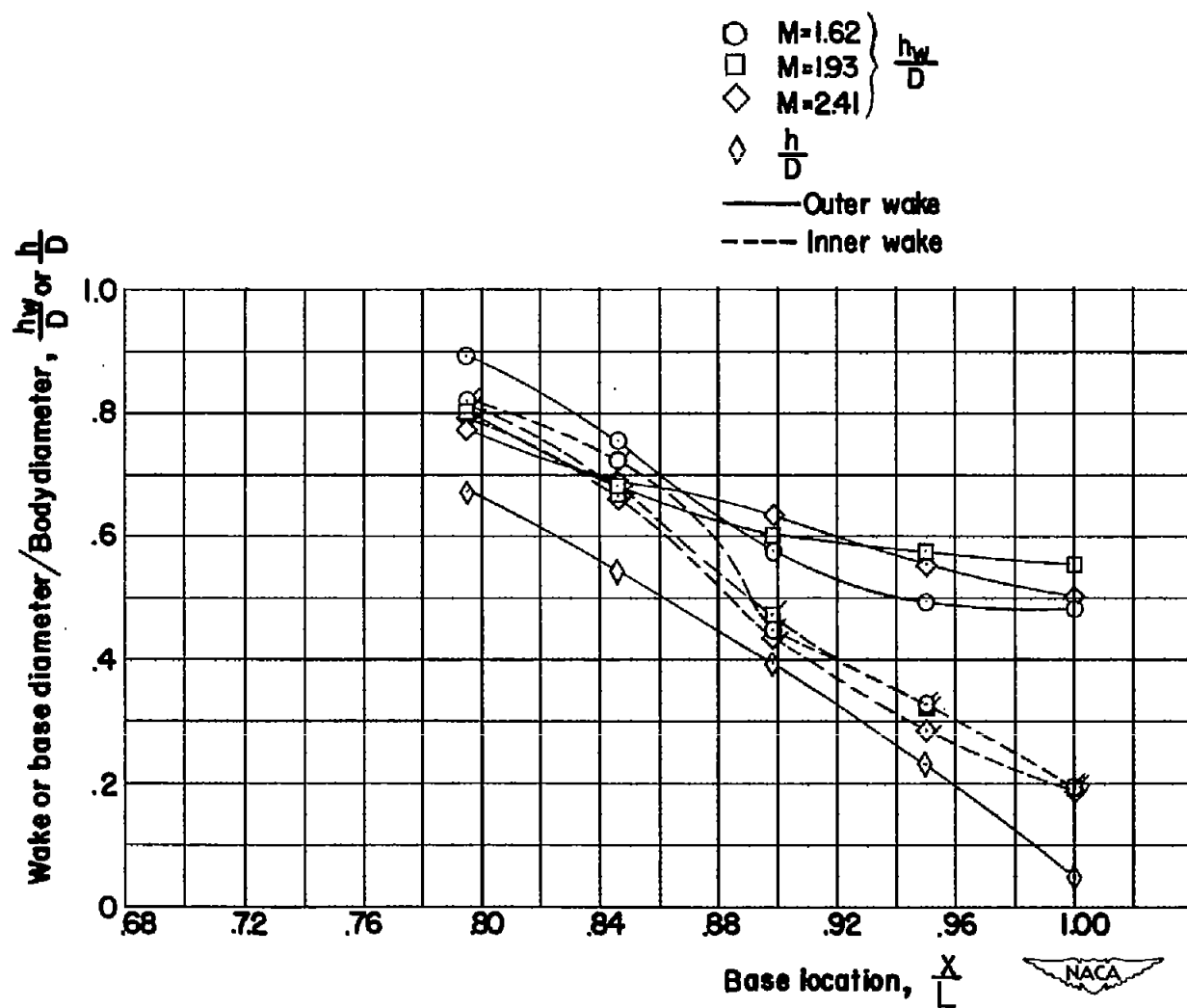
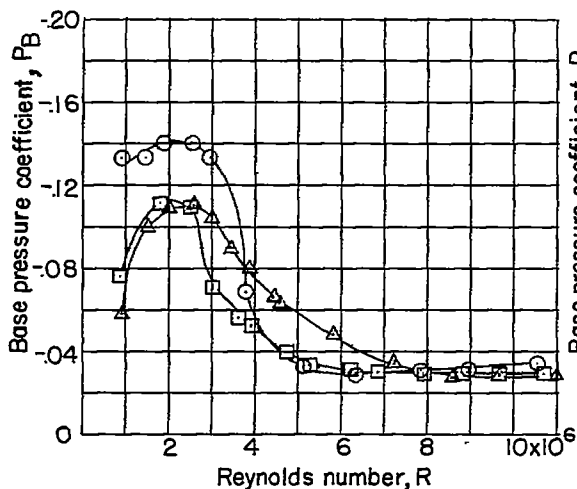
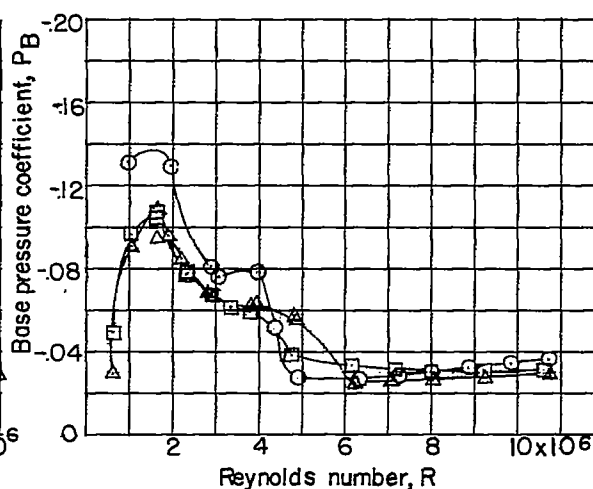


Figure 30.- Wake measurements at each base for the various cut-off lengths of the finned parabolic body.

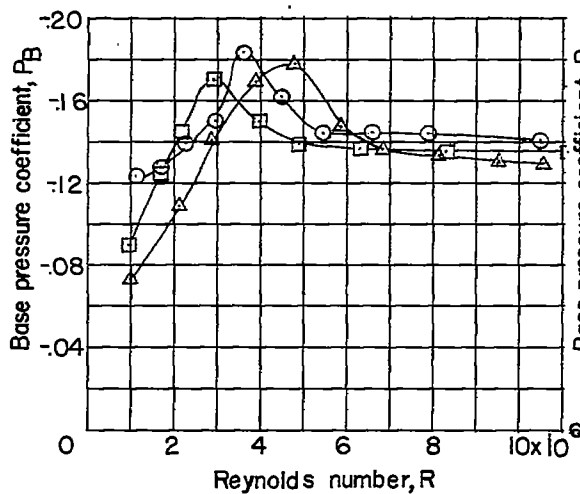


(a) Cusp base.

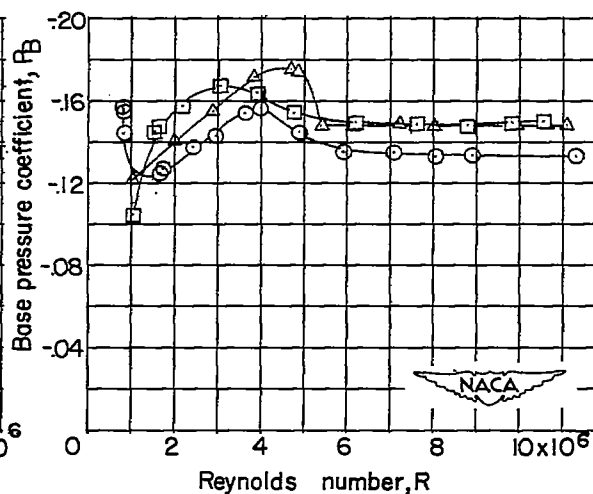


(b) Conical base.

□ Conical nose  
 △ Ogive nose  
 ○ Radome nose



(c) Boattail base.



(d) Cylindrical base.

Figure 31.- Variation of base pressure with Reynolds number at  $M = 1.62$  for the unfinned body with varying nose and base shapes.

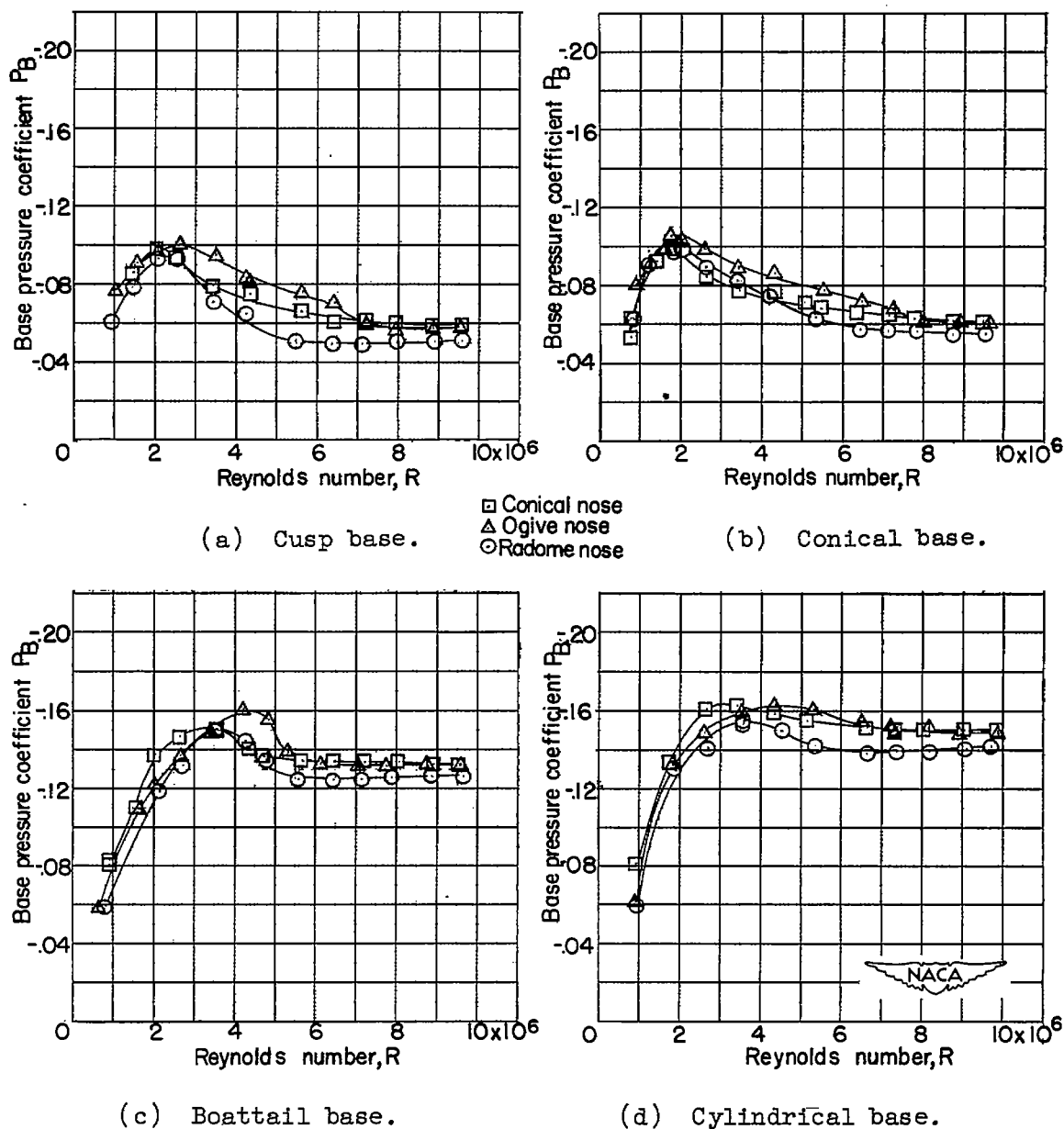


Figure 32.- Variation of base pressure with Reynolds number at  $M = 1.93$  for the unfinned body with varying nose and base shapes.

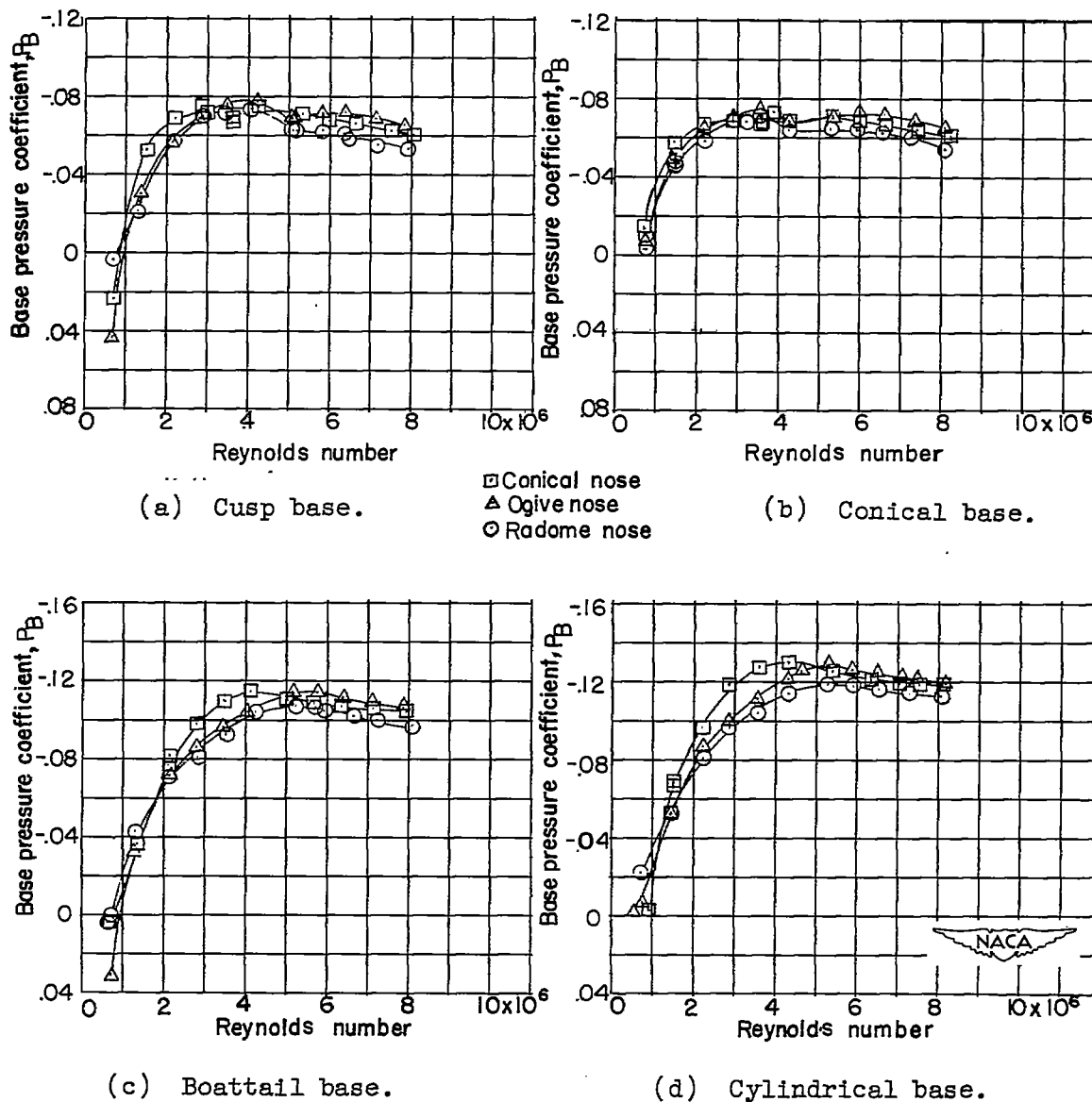


Figure 33.- Variation of base pressure with Reynolds number at  $M = 2.41$  for the unfinned body with varying nose and base shapes.

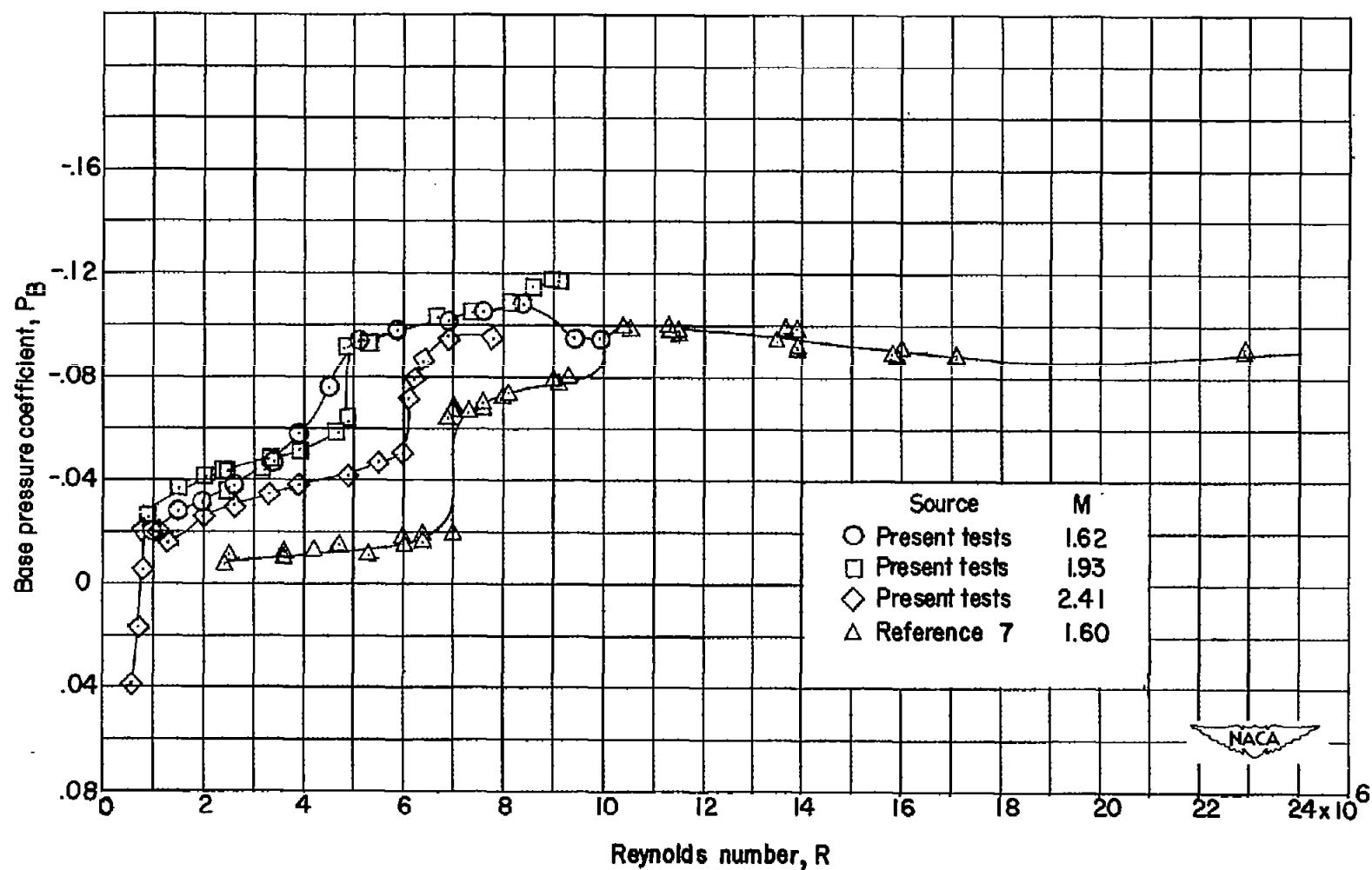
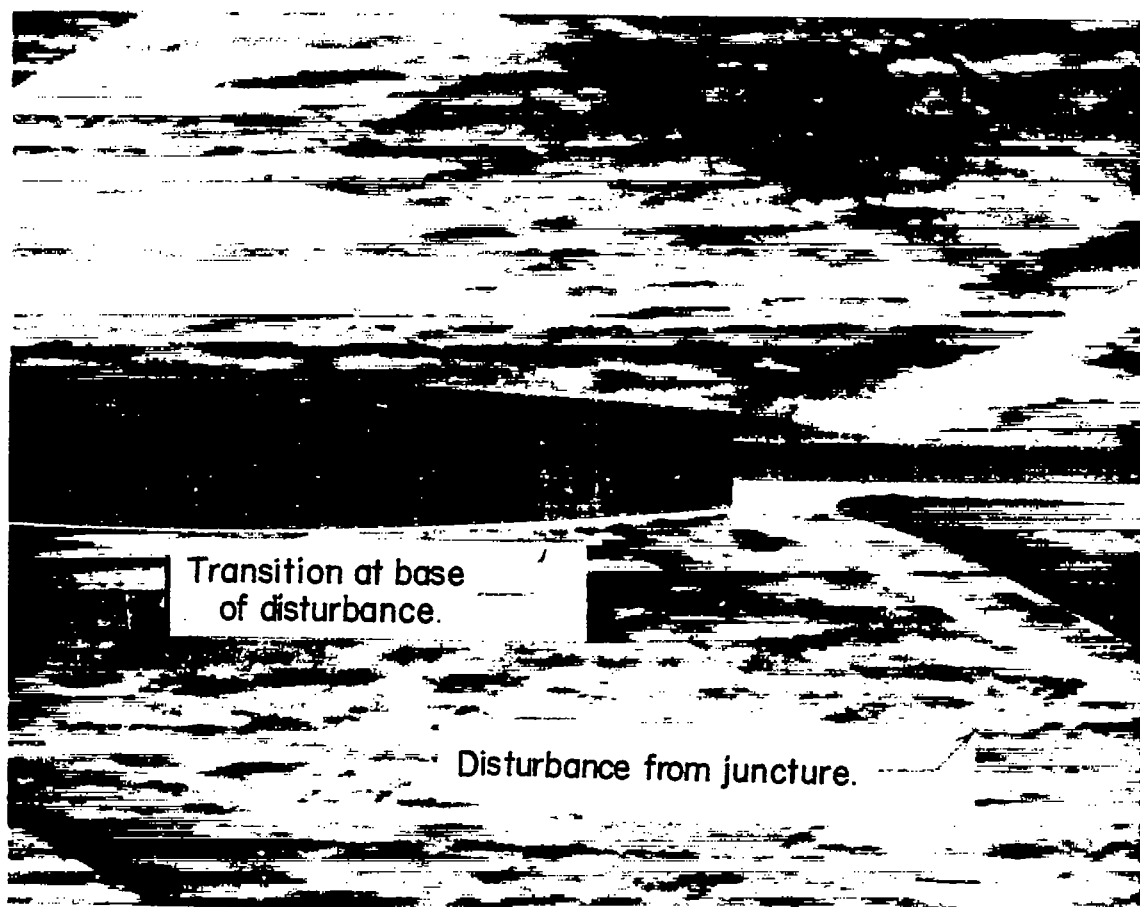
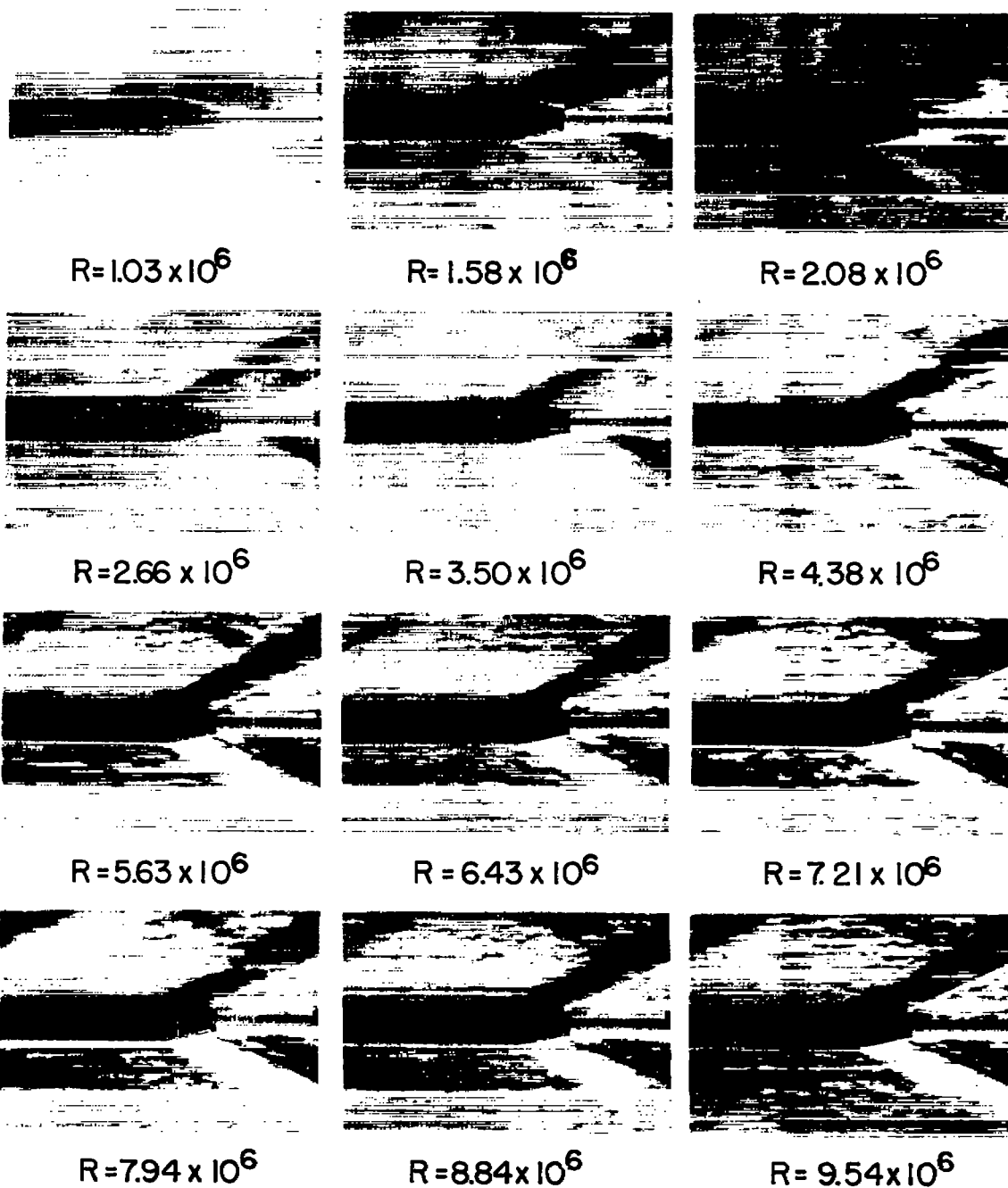


Figure 34.- Variation of base pressure with Reynolds number for base A of the unfinned parabolic body.



NACA  
L-77012

Figure 35.- Schlieren photograph showing asymmetrical transition occurring at  $M = 1.93$  and  $R = 8.55 \times 10^6$  for base A of the parabolic body as a result of small imperfections at the juncture of the base and center section.



NACA  
L-77013

Figure 36.- Effect of increasing Reynolds number upon the base phenomena at  $M = 1.93$  for the configuration with ogive nose and cusp base.

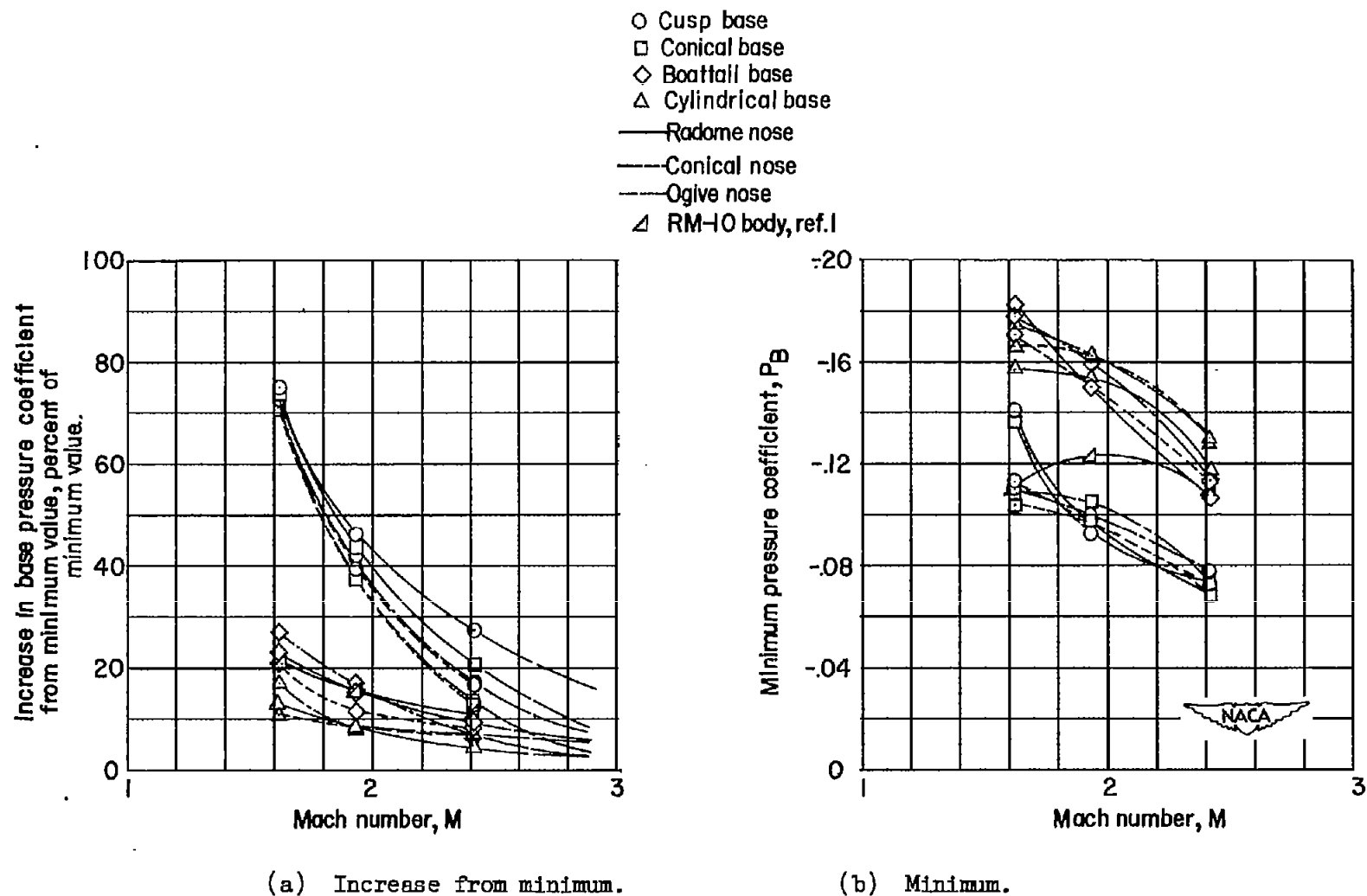


Figure 37.- Effect of Mach number upon the minimum base pressure and the increase from the minimum base pressure for various unfinned configurations.



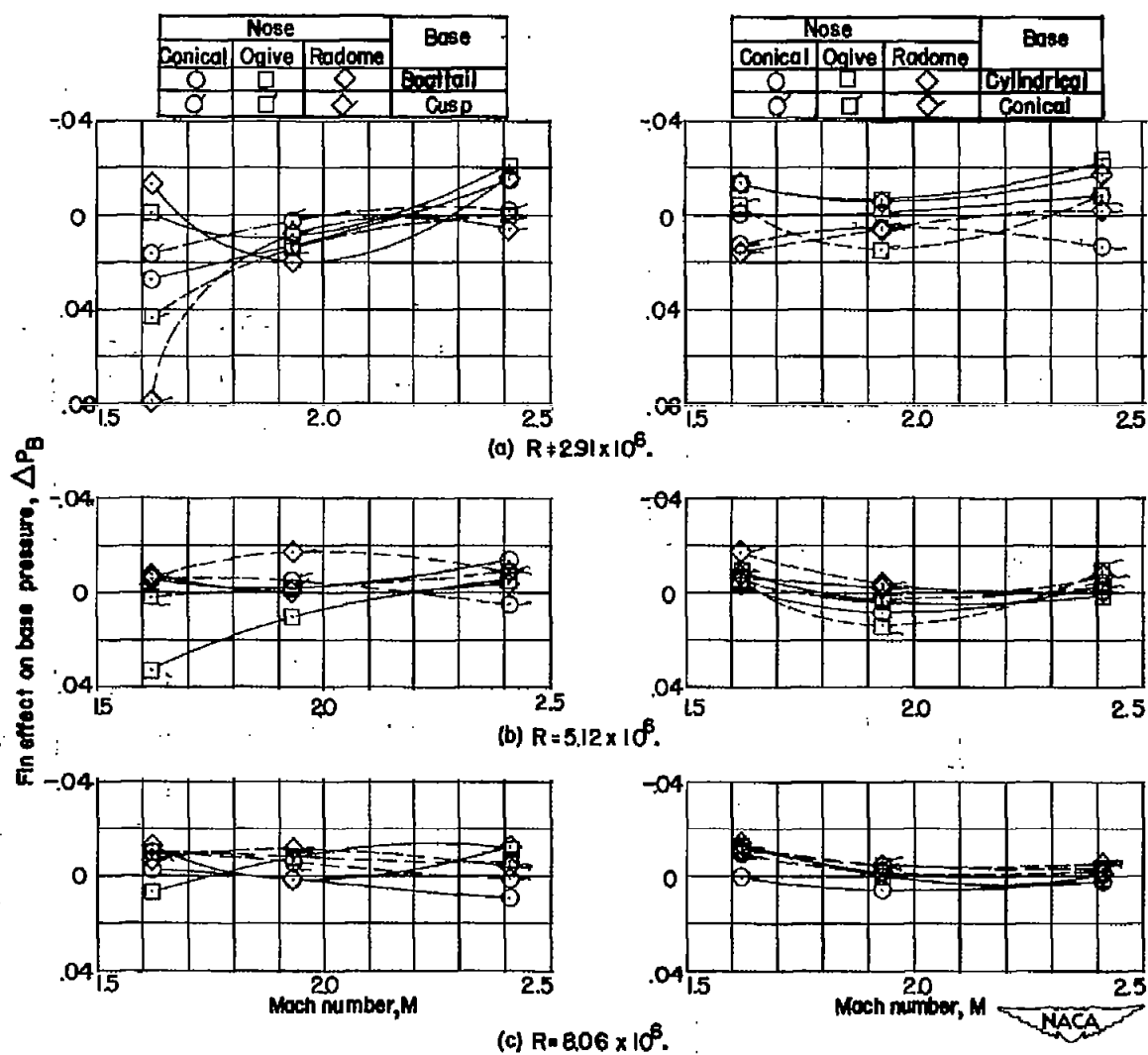


Figure 38.- Fin effects upon base pressure for the body having various nose and base shapes.

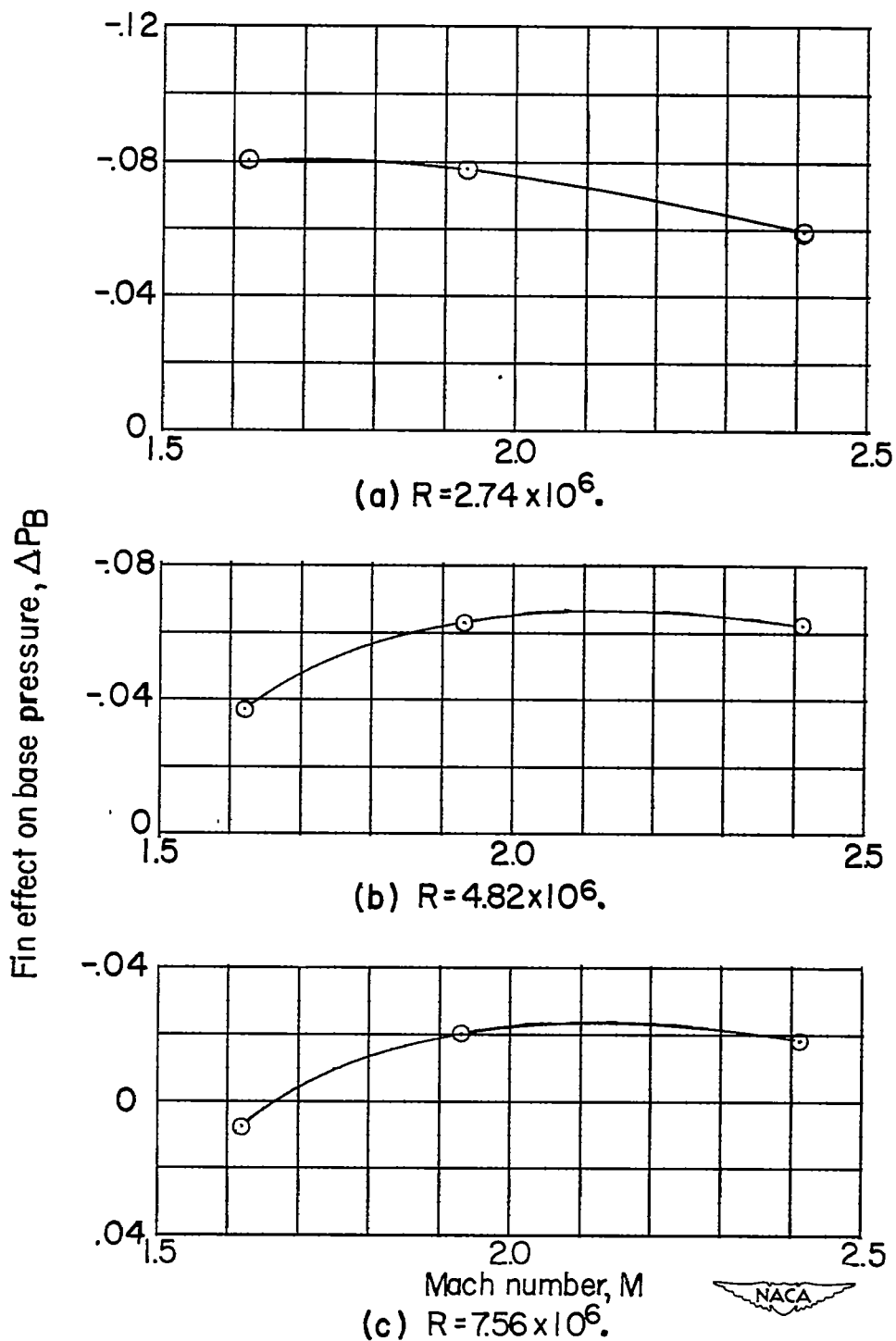


Figure 39.- Fin effects upon base pressure for base A of the parabolic body.

	Base	$R \times 10^{-6}$	
○	A	7.56	Parabolic body
□	B	8.06	
◇	C	8.54	
△	D	9.03	
▽	E	9.52	
◐	Cusp	8.06	Ogive nose
◑	Boattail	8.06	

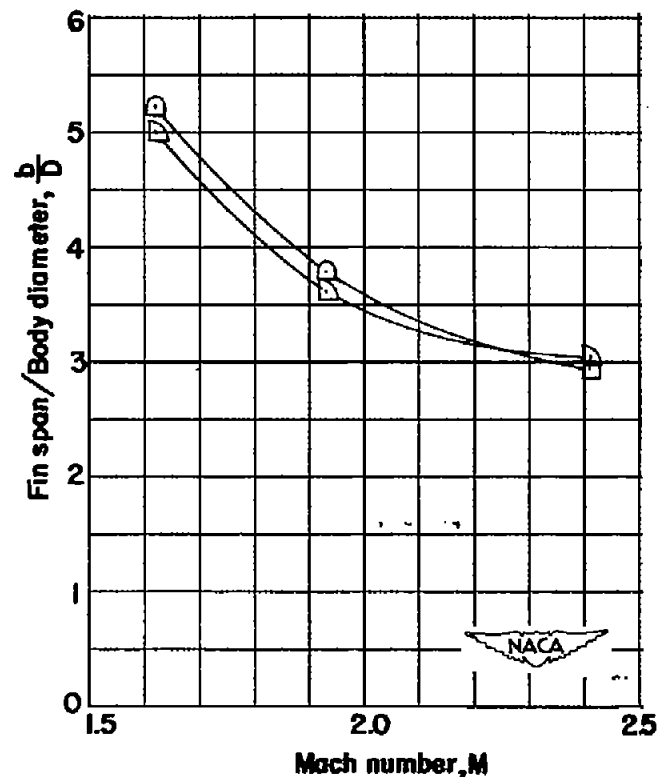
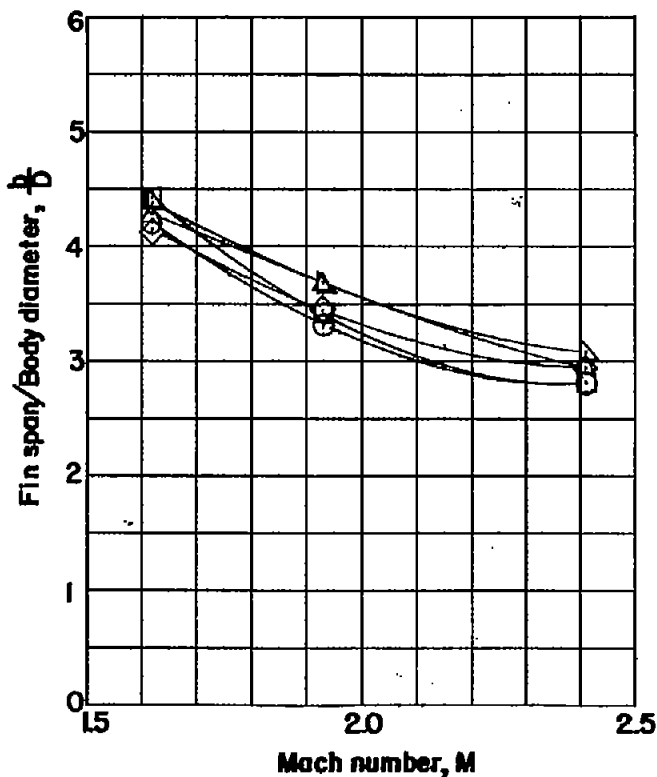


Figure 40.- An approximation of the minimum ratio of fin span to body diameter corresponding to the fin effects of the present tests.